PHILOSOPHICAL TRANSACTIONS OF THE ROYAL SOCIETY A MATHEMATICAL, PHYSICAL & ENGINEERING SCIENCES

Sea-Ice Topography of the Arctic Ocean in the Region 70 degrees W to 25 degrees E

P. Wadhams

Phil. Trans. R. Soc. Lond. A 1981 **302**, 45-85
doi: 10.1098/rsta.1981.0157

SEA-ICE TOPOGRAPHY OF THE ARCTIC OCEAN IN THE REGION 70° W TO 25° E

By P. WADHAMS

Scott Polar Research Institute, University of Cambridge, Cambridge CB2 1ER, U.K.

(*Communicated by Sir George Deacon, F.R.S. – Received* 1 *July* 1980)

CONTENTS

In October 1976 a cooperative experiment was made to survey the sea-ice topography in the European sector of the Arctic Ocean. H.M. submarine *Sovereign* acquired 4000 km of ice draft data by using an upward-looking sonar, while a Canadian Forces aircraft flew along the submarine's track and acquired 2200 km of ice elevation data by using a laser profilometer. The two types of profile were processed in corresponding 100 km section lengths, and the following statistical analyses and comparisons were made:

(i) *Probability density functions of ice draft and elevation.* Each distribution shows a peak for young ice and for undeformed multi-year ice. At large ice thicknesses the distributions take the analytical form of a negative exponential. The mean drafts enable two distinct geographical ice régimes to be identified. There is an 'offshore zone' of very heavy pressure ridging extending up to 400 km from the coasts of Ellesmere Island and of north Greenland, with mean ice draft in the range 5.0 to 7.5 m, while out in the central Arctic Ocean the mean ice draft is lower (3.9–5.1 m) and the characteristics of the ice cover remain homogeneous over a length scale of 1000 km. The transition between the two régimes is abrupt, taking place in less than 25 km. Data from the same part of the central Arctic taken in March 1971 showed a mean ice draft 0.3 m lower, while data from the central Beaufort Sea showed a mean draft more than 0.8 m lower.

(ii) *Level ice distributions.* Ice with a local gradient of less than 1 in 40 was defined as level ice, and used as an indicator of the quantity and thickness distribution of undeformed (i.e. thermodynamically grown) ice in the Arctic Ocean. The distribution has a mode at 3.0–3.1 m draft, and level-ice percentages are in the range 30–40 (bottom side) and 70–80 (top side) in the offshore zone, and 45–55 (bottom) and 85–95 (top) in the central Arctic. Thus about half of the Arctic ice cover consists of deformed ice.

(iii) *Pressure ridge spacings.* The spacings of ridge keels fit a negative exponential distribution, characteristic of randomness, except at close spacings where there is a deficit of keels (explained as a geometrical effect) and at very large spacings where there is an excess (due to the contribution of polynyas). The distribution of sail spacings exhibits these two effects, but also differs from a random distribution at moderate sail separations.

(iv) *Ridge elevations and drafts.* Keel drafts fit a law of form $P(h)\,\mathrm{d}h \propto \exp(-\lambda h^2)\,\mathrm{d}h$, except for an excess of keels at drafts beyond 20 m. There is a positive correlation between mean keel draft and keel frequency. There are 3.5–4.5 keels per kilometre with draft exceeding 9 m in the offshore zone and 2–3 in the central Arctic. Sail elevations fit a law of form $P(h)\,\mathrm{d}h \propto \exp(-\lambda h)\,\mathrm{d}h$, with a positive correlation between mean sail elevation and sail frequency. The sail elevation and ice elevation distributions can be related by assuming that all thick ice is contained in pressure ridges of triangular cross section.

(v) *Keel–sail comparison.* For the 21 corresponding 100 km sections there are positive correlations between mean sail height and mean keel draft, and between keel frequency and sail frequency. From these it is possible to convert a sail distribution (computed from a laser profile) into a keel distribution, enabling sea ice bulk characteristics to be derived from airborne surveys alone.

(vi) *Leads and polynyas.* A lead was defined as a continuous sequence of depth points greater than 5 m long and not exceeding 1 m draft. The number density $n(d)$ of leads per kilometre of width d m fits the power law $n(d) = 15\,d^{-2}$. Exceptionally wide leads were concentrated in the offshore zone and in the marginal ice zone close to the open water of the Greenland Sea.

Introduction

In October 1976 H.M. nuclear submarine *Sovereign* made an under-ice cruise in the Arctic Ocean during which she acquired an upward-looking sonar profile 4000 km long of the ice under-side. At the same time an Argus patrol aircraft of Maritime Command, Canadian Forces, operated in concert with *Sovereign* and obtained a laser profile of the top surface of the ice along 2200 km of *Sovereign's* route. A statistical analysis of corresponding sections of the sonar and laser profiles yields the relation between the distributions of ice draft and elevation and of the spacings and elevations of keels and sails. Such an analysis was made for the first 1000 km of the joint profile in Wadhams (1980). The present paper extends the analysis to

cover the entire length of the submarine track, and considers some further statistical aspects not dealt with in the earlier paper. The results of other experiments made during this joint operation have been reported by Dunbar (1978, 1979), Lowry & Wadhams (1979), Wadhams (1977, 1978*a*, *b*), Wadhams *et al.* (1979), Wadhams & Lowry (1977) and Walker & Wadhams (1979).

The route

Figure 1 shows the track of *Sovereign* within the Arctic Basin. She sailed from Devonport on 1 October 1976 and after working in the East Greenland Current she began her profiling track at A (81° N, 00° W) on 18 October at 2230 G.M.T. The first leg, the results of which are reported in Wadhams (1980), ended at B (84° 50′ N, 70° W) on 21 October at 1600 G.M.T. This leg covers the heavily ridged ice zone off the north coast of Greenland where the prevailing surface current system has a shoreward component and so generates strong convergent and shear stresses on the ice cover. The second leg BC ended at the North Pole on 23 October at 0720 G.M.T. During this leg the submarine crossed the Lomonosov Ridge, which marks the approximate boundary between the Beaufort Gyre and the Trans-Polar Drift Stream, although the boundary position is not well defined and varies greatly with time. From the Pole *Sovereign* returned southward along the 11° E meridian, which is close to the 6–7° E longitude maintained by H.M.S. *Dreadnought* during her 1971 passage to the Pole; thus the ice statistics for this region can be directly compared with those of *Dreadnought* (Swithinbank, 1972; Williams *et al.* 1975). *Sovereign* diverted to run several zigzag tracks across the Arctic mid-Oceanic Ridge for hydrographic purposes, then from E to A she reproduced her outward track a few kilometres to the south. The offset was to obtain additional bathymetry, but the tracks are close enough to be statistically comparable and hence a test can be made of whether any parameters in the ice distributions vary significantly over the 11 day lag between the profiles AE and EA.

The Argus flew track AB on 19 October in ideal atmospheric conditions and obtained a complete laser profile. On 21 October it made a flight to B in order to make a rendezvous with *Sovereign* and to profile the local topography. It was then delayed at Thule by bad weather until 26 October, when it flew along the track BC and southward from C along the 11° E meridian. It did not follow the submarine zigzags but continued along 11° E to 84° 45′ N before returning to base. Some data loss occurred during this flight owing to undercast fog.

The time comparison for the three corresponding sections of track is as follows:

	submarine				aircraft			
AB	18 Oct.	15h50	to 21 Oct.	16h05	19 Oct.	18h11	to 19 Oct.	21h11
BC	21	19h42	23	07h20	26	16h28	26	18h27
CD	23	15h10	24	08h50	26	18h27	26	20h24

Thus the mismatch in time was least for section AB, where a coincidence was obtained at one point (F in figure 1). For sections BC and CD the submarine led the aircraft by between $2\frac{1}{2}$ and 5 days.

Both the submarine and the aircraft were equipped with inertial navigation systems, and the submarine was able to check her system against satellite and Omega fixes during eight surfacings through polynyas (the dated black dots in figure 1). The accuracy of positioning was therefore very good. Fixes were supplied at 15 minute intervals by the submarine and at

PHILOSOPHICAL TRANSACTIONS OF THE ROYAL SOCIETY A MATHEMATICAL, PHYSICAL & ENGINEERING SCIENCES

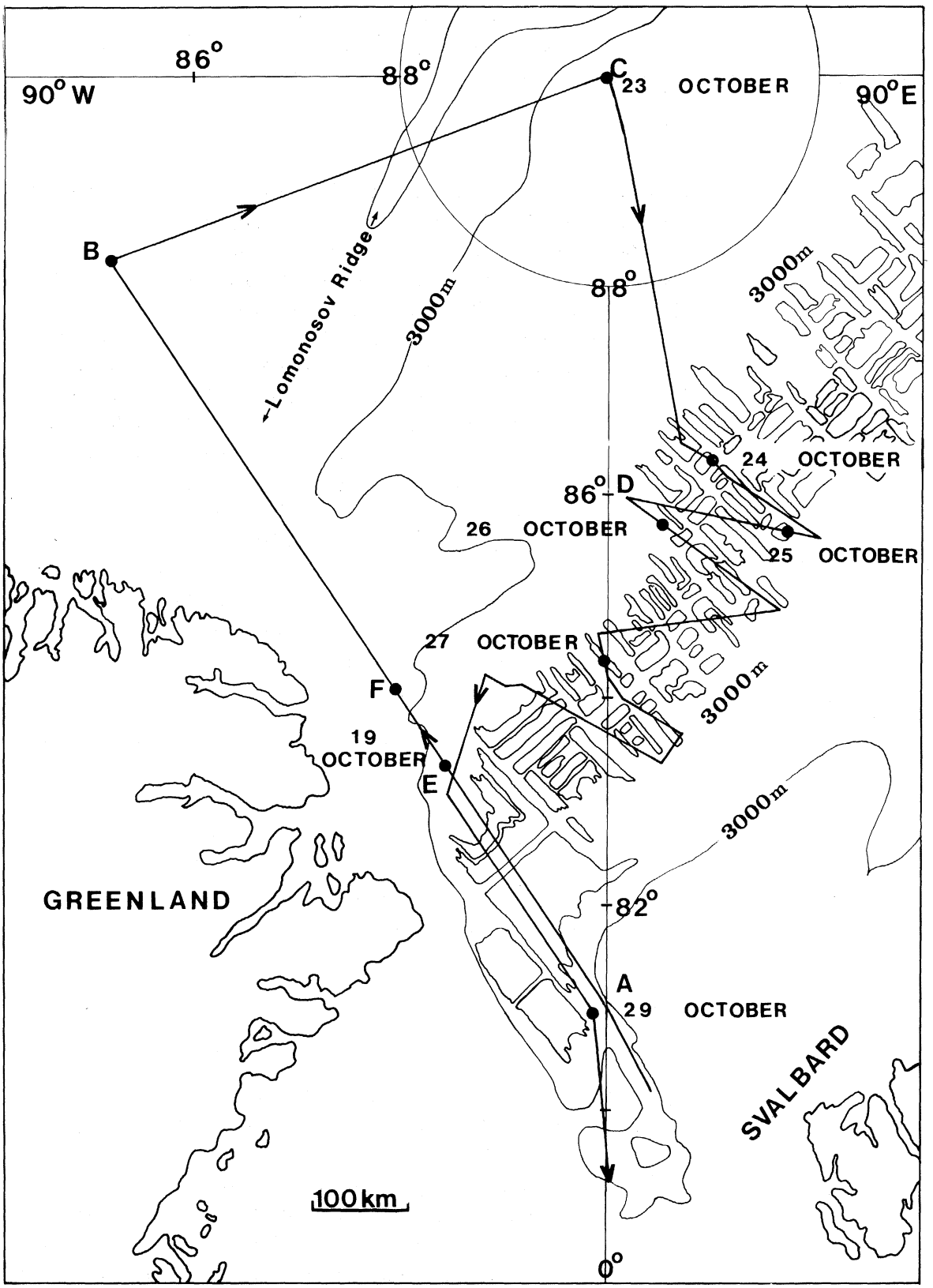

FIGURE 1. The track of H.M.S. *Sovereign* in the Arctic Ocean, October 1976. The black dots are positions of surfacings. For meaning of letters see text.

10 minute intervals by the aircraft, from which the respective tracks were computed with the use of a great circle program to interpolate between fixes. A plot of the tracks showed that excellent coincidence was obtained except during leg AB, when the aircraft kept persistently 2 km to the south of the submarine track; this is probably because of the frequent changes of course necessary to maintain a great circle track that is other than N–S. We assume that all given fixes are accurate; in fact the absolute error in each fix is at least ± 2 km, although the relative error (error in computing distances between successive fixes) is much smaller.

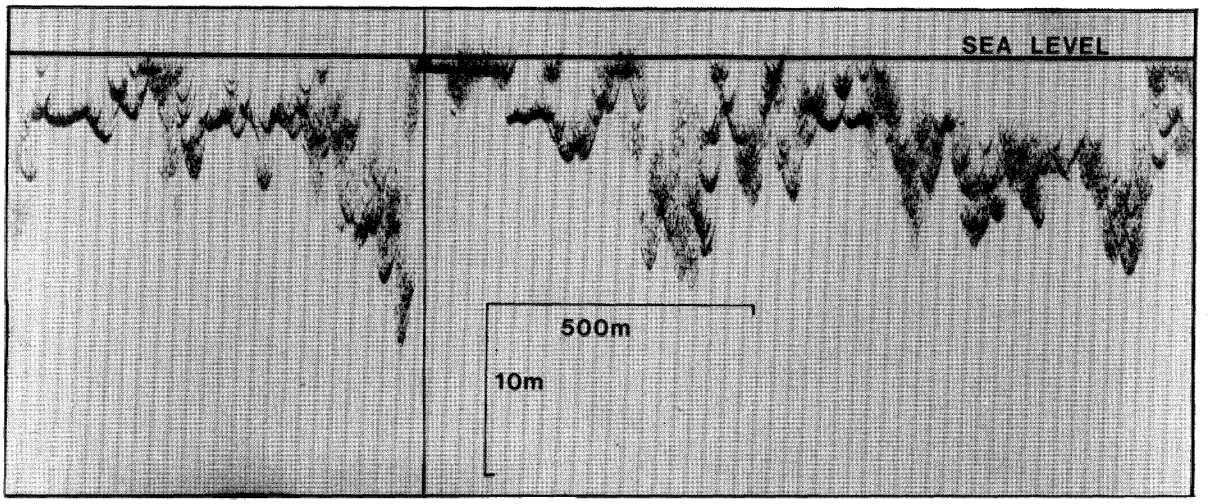

FIGURE 2. A section of under-ice profile.

DATA RECORDING AND PROCESSING

Submarine

The submarine sonar profile was recorded on teledeltos paper by using a Kelvin Hughes MS45 echo sounder feeding a 45 kHz transducer with overall beamwidths to the 3 dB points of 17° fore and aft, and 5° athwartships. The transducer was mounted on the upper casing of the submarine near the bow. The narrow sideways beamwidth ensures that ice features to the side of the track are not recorded, while the wider fore-and-aft beamwidth introduces an error in the profile which can, in principle, be corrected. The chart record scales were 2 m: 10 mm vertically and 1 minute: 75 mm horizontally. The chart was marked every 15 minutes and all speed and course changes recorded as they occurred. There was a small loss of data every 6 hours during roll changes. Figure 2 shows a typical piece of record.

The envelope of the sonar profile was digitized at approximately 1 m intervals by using a curve follower, and corrected for varying submarine speed and for submarine depth variations. If no speed changes occurred during a given 15 minute interval, the speed for that interval was calculated from the fixes marking its beginning and end. If a speed change occurred, the times of the beginning and end of the speed alteration were noted and the speed during the alteration was continuously computed on the assumption of a quadratic acceleration or deceleration. The depth variations were obtained by frequently digitizing a 'sea level profile' with sea level points taken either from open water cracks (which gave characteristic multiple sonar echoes) or from refrozen leads and polynyas with the assumption that the ice draft was

similar to that encountered at the nearest surfacing position. The submarine's depth-keeping on autopilot was good to ± 20 cm but with a period comparable with the interval between sea level fixes. Thus each digitized depth point has an absolute accuracy of about ± 20 cm, and we assume that the error is a random rather than a bias error.

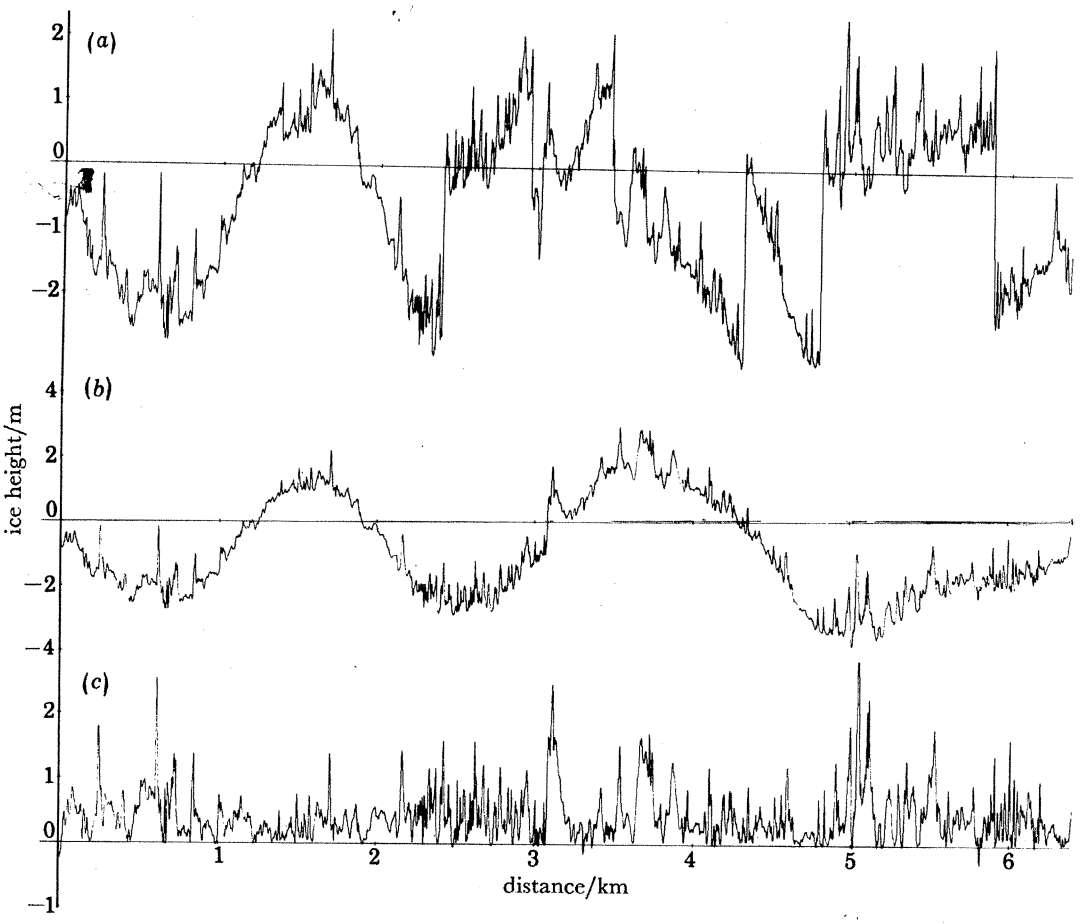

FIGURE 3. A laser profile of sea ice: (*a*) as recorded; (*b*) with phase jumps removed; (*c*) with aircraft porpoising removed.

The corrected depth points were then linearly interpolated to a standard 1.5 m horizontal spacing, and data files for successive 15 minute intervals were concatenated until a section of total length 100 km was obtained. The geographical length of such a section is usually more than 100 km, because of loss of data, but it can be less on occasions when the submarine ran a local search pattern in quest of a polynya for surfacing. The 100 km section was then the basis for all subsequent statistical analyses. This length was chosen as being large enough to generate reliable statistics while short enough to reveal genuine changes in ice properties from section to section; a shorter section length of 50 km was used in Wadhams & Horne (1980) to analyse sonar profiles from the Beaufort Sea.

Aircraft

The laser profile was obtained by using a Spectra-Physics Geodolite 3A profilometer which uses an amplitude-modulated continuous He–Ne laser beam (Ketchum 1971). Profiles were

recorded on analogue magnetic tape and on an ultraviolet chart recorder. The modulation frequency used was such that a full scale deflexion, caused by a single cycle of phase shift between transmitted and reflected beams, corresponds to 20 feet (6.096 m) of terrain elevation. Since the signal:noise ratio in the tape recorder was 48 dB the noise signal in the tape record represents some 3 cm of 'elevation'. The aircraft height was normally 1220 m and the speed between 80 and 100 m s^{-1}. Analogue-to-digital conversion of the tape record was made at 0.01 s intervals through a 200 Hz analogue low-pass filter to remove energy above the Nyquist frequency.

TABLE 1. POSITIONS OF SECTIONS USED IN STATISTICAL ANALYSIS

section†		latitude N	longitude	data length/km submarine	aircraft
1	starts	81° 00.0′	00° 00 W′		
	ends	81 43.1	03 12 W	80	97
2		82 22.6	07 04 W	89	96
3		83 00.0	11 48 W	92	97
4		83 35.9	17 30 W	104	99
5		84 05.8	24 02 W	90	96
6		84 30.5	31 55 W	84	100
7		84 47.0	40 51 W	88	98
8		84 57.9	50 32 W	62	94
9		84 58.9	60 37 W	74	100
10		84 50.0	70 00 W	43	86
11	starts	84 53.3	69 24.8 W		
	ends	85 45.9	69 57.3 W	95	40
12		86 45.1	70 01.2 W	100	85
13		87 42.0	70 00.1 W	100	90
14		88 54.2	70 00.0 W	101	134
15		89 49.8	70 00.0 W	101	68
16		89 56.9	60 W (Pole)	100	54
17		89 31.6	16 35 E	101	77
18		88 34.5	11 50 E	100	104
19		87 39.5	11 18.8 E	101	95
20		86 45.0	11 10 E	100	97
21		86 06.0	15 26 E	101	48
22		85 23.3	22 30.8 E	100	
23		85 28.0	18 03.0 E	103	
24		85 52.4	6 39.1 E	100	
25		85 38.1	7 25.1 E	99	
26		84 56.4	15 17.4 E	101	
27		84 38.8	12 58.0 E	99	
28		84 39.5	3 43.9 E	104	
29		84 11.7	00 10.0 W	102	
30		84 01.9	01 03.8 E	102	
31		83 29.7	05 46.7 E	98	
32		83 42.1	00 50.4 W	100	
33		84 06.2	11 23.0 W	102	
34		83 16.0	12 18.0 W	95	
35		82 25.2	08 51.0 W	102	
36		81 43.0	04 28.4 W	101	
37		80 58.8	00 51.6 W	101	
38		80 09.3	00 17.8 W	99	
39		78 53.4	00 00.0 W	136	
			total	3750	1853

† Except for nos 1 and 11 the sections start where the preceding one ends.

PHILOSOPHICAL TRANSACTIONS OF THE ROYAL SOCIETY A MATHEMATICAL, PHYSICAL & ENGINEERING SCIENCES

Figure 3 (top) shows a laser profile as first digitized. Since it is simply a profile of range between the aircraft and the terrain the actual ice surface profile is modulated by the profile of aircraft porpoising (usually oscillations of 1–4 km wavelength and several metres amplitude) as well as by occasional noise spikes and by phase jumps, which are 10 ft (3.048 m) (180°) steps occurring automatically when the phase shift reaches 0° or 360°. The phase jumps are not quite instantaneous nor are they always of exactly 10 ft (3.048 m). The data correction

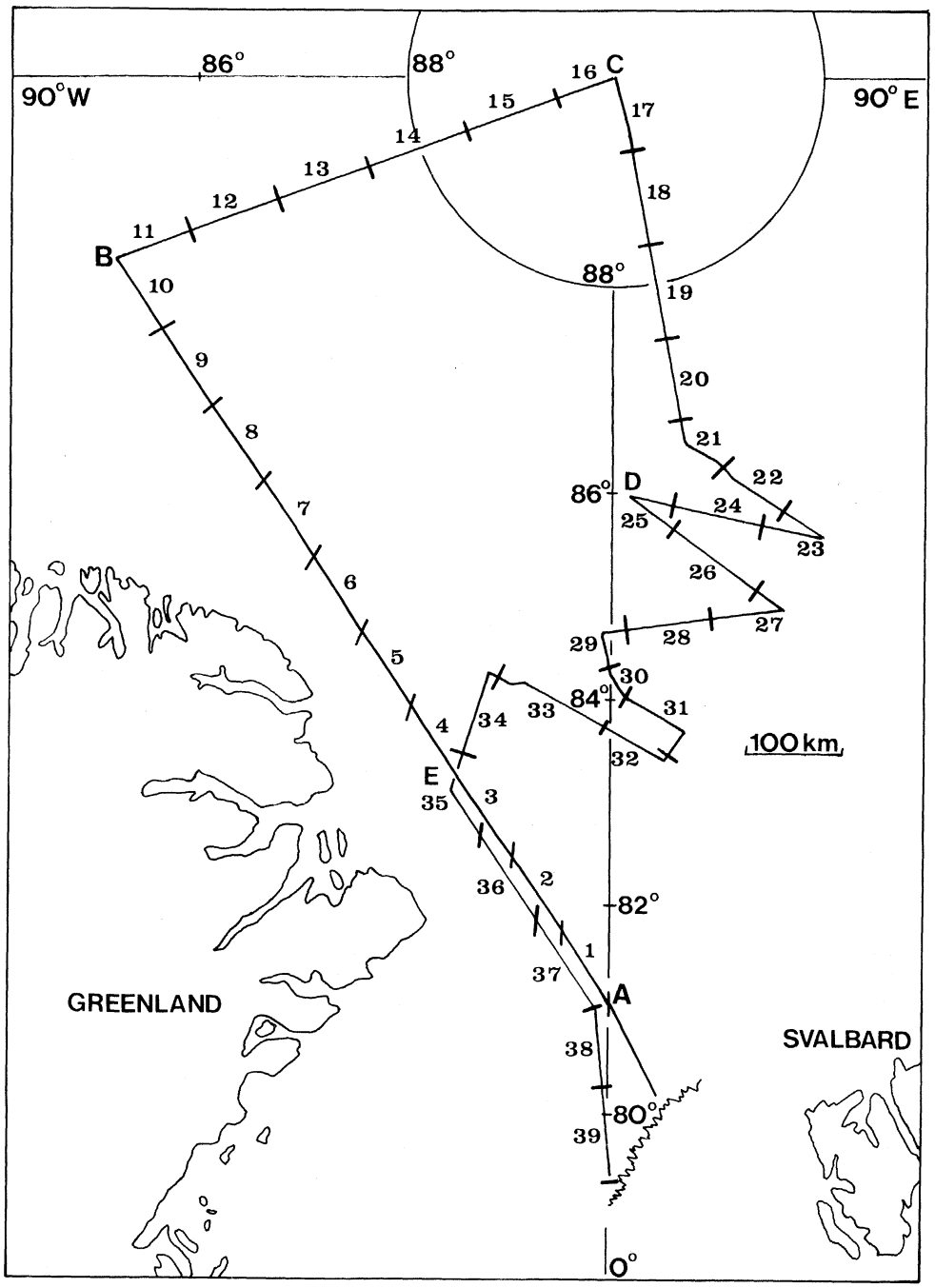

FIGURE 4. Position of 100 km sections used in statistical analysis.

PHILOSOPHICAL TRANSACTIONS OF THE ROYAL SOCIETY A MATHEMATICAL, PHYSICAL & ENGINEERING SCIENCES

problem is therefore serious. Porpoising cannot be removed by a simple filter, since a laser profile is non-Gaussian, although Hibler (1972) used a complex three-stage filtering technique successfully. Instead a manual interactive graphics technique was used. This was originally developed by Lowry & Brochu (1978) and modified for the Cambridge University PDP11/45-Vector General system by Holyer *et al.* (1977). The raw profile is displayed in sections of length 2000 points on a graphics terminal; phase shifts and noise spikes are replaced by short horizontal line segments (to give a profile similar to figure 3, centre); and then a piecewise straight line profile of porpoising is inserted by using the light pen to connect data points on level ice surfaces. The piecewise profile is smoothed by filtering and subtracted from the original profile, leaving a corrected profile as shown in figure 3 (bottom). The zero level for this profile is thus a mean freeboard of undeformed ice floes, rather than sea level itself; this was necessary because polynyas were too far apart to yield an infallible zero level profile against the influence of aircraft porpoising.

The mean data point spacing for each 2000 point file was calculated from position fixes. Then, files (each of length 1.6–2 km) were concatenated to fit the geographical section intervals as defined by the submarine profiles. It was found that the laser data covered the first 21 sections, although section 21 (laser) does not correspond exactly with section 21 (submarine) because the submarine began zig-zagging while the aircraft continued on a southward course. The positions of start and finish for the 100 km sections are given in table 1; the first ten sections are those reported in Wadhams (1980). The geographical position of the sections is shown in figure 4.

Beamwidth correction

The nominal beamwidths of the upward-looking echo sounder were 17° in the fore-and-aft plane and 5° athwartships. By assuming that the effect of the athwartships beamwidth is negligible we can make a beamwidth correction which is more reliable than that used for the *Dreadnought* profile, where the beam was wide in both planes. The fore-and-aft beamwidth to use for profile corrections is that within which an identifiable echo is painted on the echo sounder recorder. To determine this, a large number of hyperbolae were measured from point reflectors (e.g. edges of floes, rafted blocks within polynyas, narrow cracks) on sections of record taken at submerged speeds between 6 and 18 knots (3.1–9.3 m s^{-1}). If the point reflector lies at (x_0, D) and the transducer is at a depth H, then an echo is first received when the transducer reaches the point $(x_0 - (H-D)\tan\theta, H)$, where θ is the effective half-angle beamwidth. This neglects the travel time of the sound pulse. The apparent width W of the echo hyperbola generated by the point reflector is then given by

$$W = 2(H-D)\tan\theta. \tag{1}$$

The measurement yielded $\theta = 11.0 \pm 0.2°$, with no significant difference between profiles recorded at low and high submarine speed. This is slightly greater than the nominal 8.5° to the 3 dB level, probably owing to the large dynamic range of the recorder.

The beamwidth correction can now be made by using the equations of Harrison (1970). In the notation of figure 5, the digitized envelope is given by $(s, H-r(s))$, since the digitization of sea level is assumed correct, while the corresponding corrected depth point is $(x, H-y(x))$. The parameters x and y are related to s and r by

$$x = s - r\,\mathrm{d}r/\mathrm{d}s, \tag{2}$$

$$y = r[1-(\mathrm{d}r/\mathrm{d}s)^2]^{\frac{1}{2}}. \tag{3}$$

These equations are valid so long as dr/ds is single-valued, i.e. is not a cusp between two overlapping hyperbolae. When the equations are invalid a corrected point cannot be generated; this occurs most frequently at the trough between two close peaks. The equations are also inapplicable if the reconstruction involves an angle greater than the beamwidth of the transducer, i.e. if $y/r < \cos\theta$. In these cases the reconstructed point was placed on the edge of the beam, i.e.

$$y = r\cos\theta, \tag{4}$$

$$x = s + r\sin\theta \quad \text{if} \quad dr/ds < 0,$$
$$= s - r\sin\theta \quad \text{if} \quad dr/ds > 0, \tag{5}$$

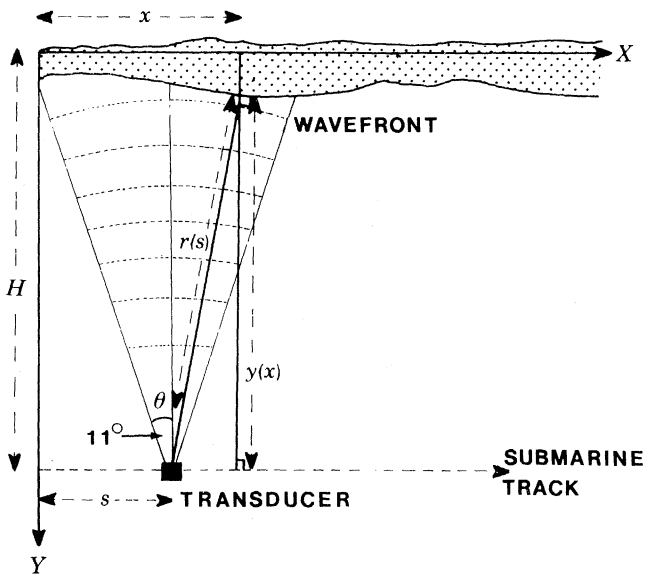

FIGURE 5. Geometry of a wide-beam echo sounder.

A major drawback of profile reconstruction, or deconvolution, is that it cannot regenerate the full depth of a trough between two peaks when that trough is obscured by two overlapping hyperbolae. A possible, although exceedingly time-consuming, technique would be to digitize each of the two hyperbolae rather than the envelope of the profile; even so the bottom of the trough is lost, although the reconstruction can proceed further down the slopes.

A second method of correcting for beamwidth effects, which avoids the problem of 'lost troughs' is to proceed in the reverse direction, that is, to take a narrow-beam ice profile and to simulate the effect of passing a wide beam over it. Calibration curves for the various statistical parameters can be drawn by applying the simulation to profile sections with widely differing ice characteristics; the corrected values for the parameters are then read off the curves. A suitable narrow-beam profile became available in 1976 when U.S.S. *Gurnard*, equipped with a sonar of 2° beamwidth, ran a 1400 km profile track in the Beaufort Sea (Wadhams & Horne 1980). A simulation was made on all 27 of the 50 km track sections reported by Wadhams & Horne, by using a 22° overall beamwidth and a transducer depth of 74.7 m so as to correspond with the *Sovereign* profile. The results are reported later in this paper.

The chief effect of beamwidth correction is to alter the probability density function of ice draft so as to reduce the mean draft. The result may still be too high, for the first method described above, but is a far better estimate than the uncorrected draft. A wide beam has no effect on the absolute draft reported for a pressure ridge keel crest, but it reduces the number of 'independent' ridges by obscuring the troughs between closely spaced ridges so that the computer does not perceive them as separate. Again the first correction method does not solve this problem, while the second does so statistically.

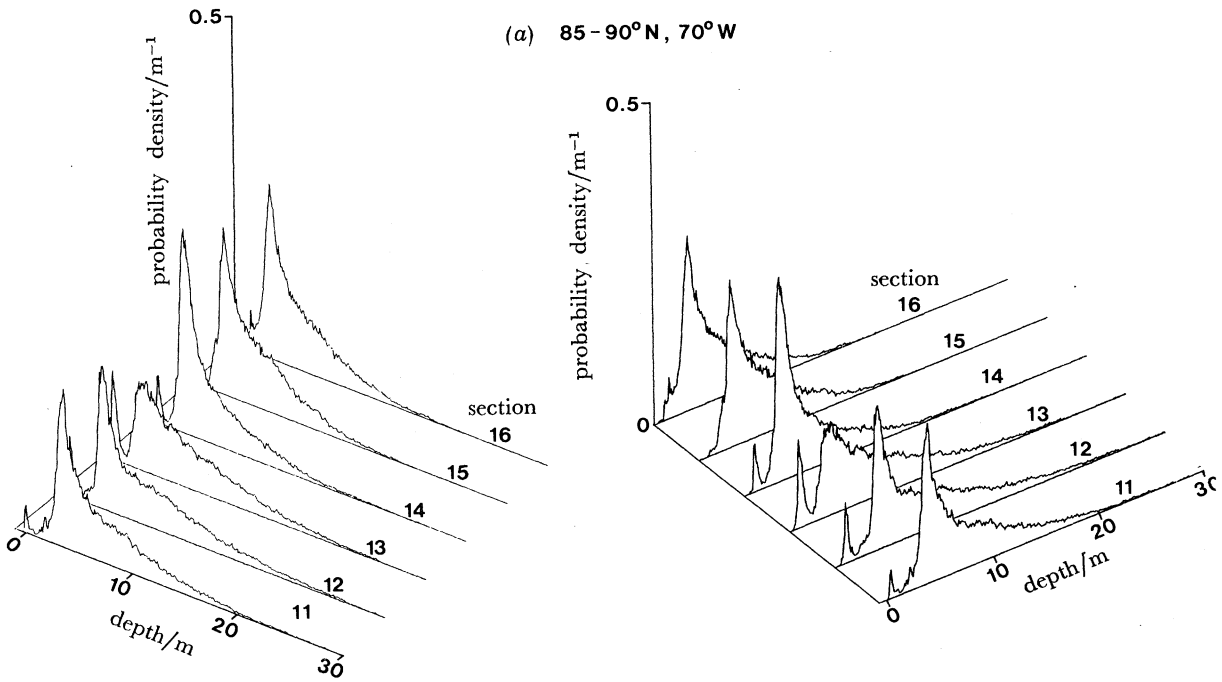

FIGURE 6(a). For description see following page.

DISTRIBUTION OF ICE DRAFT AND ELEVATION

Draft

The probability density function $P(h)$ of ice draft is defined such that $P(h)\,\mathrm{d}h$ is the probability that a random point on the ice underside has a draft between h and $h+\mathrm{d}h$. $P(h)$ is a function of time, the quantity of thin ice varying especially rapidly on a scale of days. More important, $P(h)$ is a function of the length or area scale that is used operationally to derive it. A small length of sonar profile, while defining a more exact geographical location, does not include a large enough sample of ice types to give a reliable estimate of $P(h)$; a very long record, however, may mask genuine changes in the nature of the ice cover. In Wadhams & Horne (1980) a length scale of 50 km was used, while in Wadhams (1980), and in this paper we use 100 km with further subdivision where necessary. A correction for the mean density of sea ice turns $P(h)$ into a reliable measure of $g(h)$, the ice thickness distribution function (Thorndike *et al.* 1975). This function is of great importance as both an input and an output to models of Arctic ice dynamics and thermodynamics (Coon 1980; Hibler 1979), with the distribution of

ice less than 1 m thick as the most sensitive thermodynamic parameter (Maykut 1978) since most of the vertical heat flow occurs through thin ice.

We shall first examine the probability density function uncorrected for beamwidth, which we shall call $P'(h)$, to look at variations in ice characteristics over the whole geographical area covered by the submarine. Figure 6 shows $P'(h)$ for some of the most interesting sections.

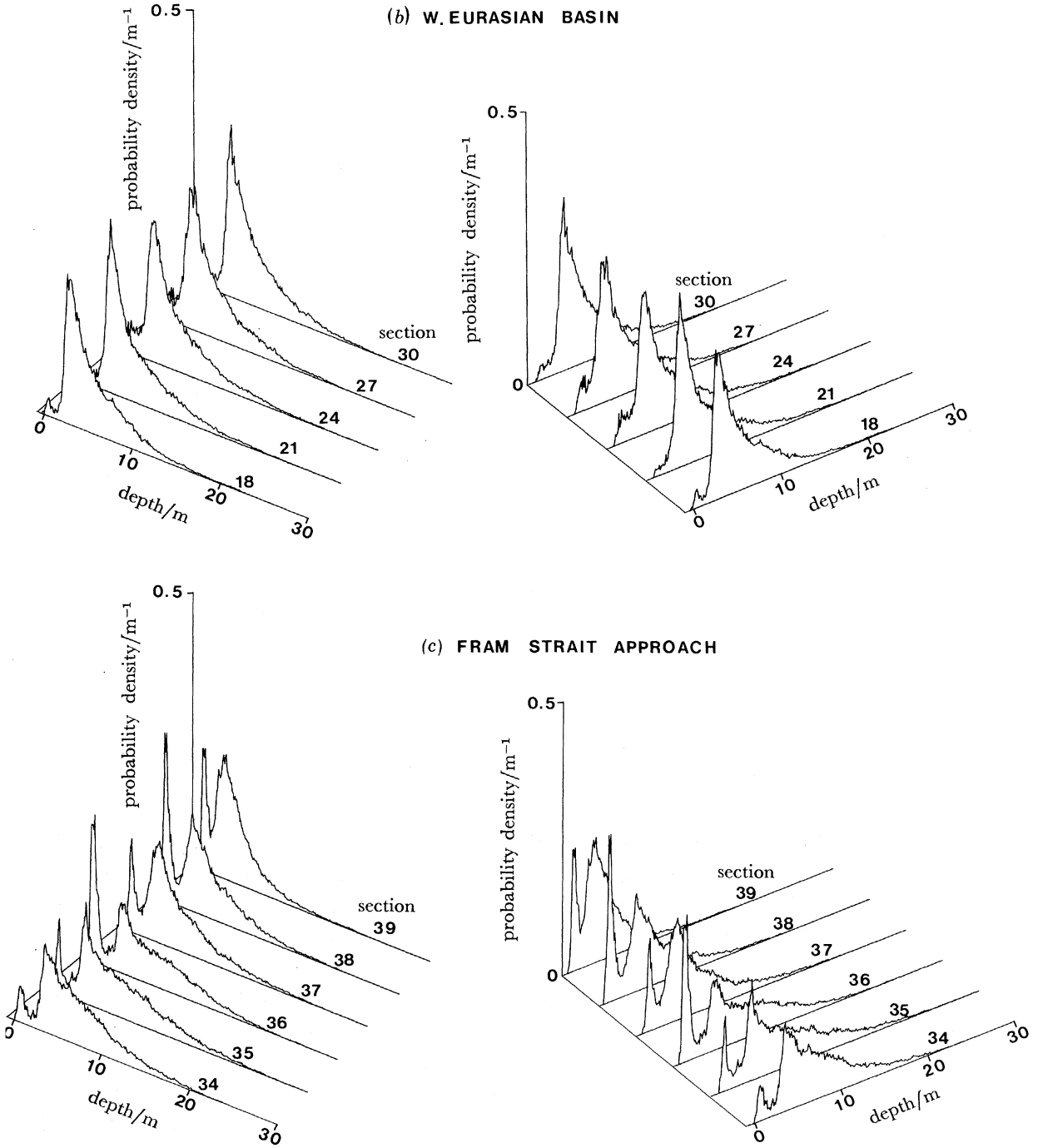

FIGURE 6. Probability density functions of ice draft, uncorrected for beamwidth: (*a*) the transect from 85 to 90° N at 70° W; (*b*) sample sections from the central Arctic régime; (*c*) the outward profile towards Fram Strait.

PHILOSOPHICAL TRANSACTIONS OF THE ROYAL SOCIETY A MATHEMATICAL, PHYSICAL & ENGINEERING SCIENCES

Figure 6*a* shows the change in $P'(h)$ along the leg BC (figure 1) from north of Ellesmere Island to the Pole. A significant change in ice conditions occurs between sections 12 and 14, in the vicinity of 87° N, with a sudden decrease in the mean ice draft. From section 14 onwards as far as section 31 the ice conditions are remarkably constant, and the ice statistics appear to be drawn from a single population; figure 6*b* gives a sample of these sections. As the track approaches the north Greenland coast again at E (figure 1) the mean ice draft increases again, until it is similar to that found by Wadhams (1980) along leg AB. Sections 34 to 39, shown in figure 6*c*, display the marked changes in ice conditions that occur along the track EA, especially

TABLE 2. ICE DRAFT DISTRIBUTION: PERCENTAGES IN DIFFERENT DRAFT BANDS; ALL DATA UNCORRECTED FOR BEAMWIDTH

section	percentage of ice < 0.5 m	0.5–2 m	2–5 m	> 5 m	mean draft/m	approximate region
1	1.8	4	29	66	6.95	leg AB (from Wadhams 1980)
2	8.6	5	27	60	6.87	
3	8.0	5	25	62	6.88	
4	12.2	8	25	54	6.04	
5	8.7	6	31	54	6.41	
6	1.9	3	28	67	7.93	
7	2.0	1	32	65	7.52	
8	1.1	3	31	65	7.51	
9	2.1	2	34	62	7.20	
10	1.3	1	21	77	8.92	
11	1.4	2	38	59	7.31	leg BC northward to Pole
12	3.6	2	36	58	7.63	
13	6.8	4	34	55	6.81	
14	2.9	4	54	39	5.22	
15	0.4	10	46	43	5.28	
16	1.4	10	48	40	5.06	North Pole
17	5.2	10	49	36	4.69	southward along 11° E
18	1.5	4	54	41	5.25	
19	1.3	4	51	44	5.48	
20	1.0	5	51	44	5.52	
21	0.6	4	53	42	5.48	first Ridge transect
22	2.8	6	52	39	5.36	
23	1.8	8	51	39	5.04	second Ridge transect
24	1.4	6	49	43	5.46	
25	1.4	5	47	47	5.88	third Ridge transect
26	1.1	5	46	48	6.02	
27	1.3	7	51	40	5.18	fourth Ridge transect
28	0.2	5	50	45	5.56	
29	1.1	6	51	41	5.31	
30	0.6	4	53	42	5.37	fifth Ridge transect
31	2.0	7	49	43	5.42	
32	4.8	4	42	49	5.79	sixth Ridge transect
33	8.5	11	34	47	5.72	
34	1.4	6	30	63	7.11	south to E
35	1.1	8	27	63	7.56	leg EA 35 ≡ 3, 36 ≡ 2, 37 ≡ 1
36	10.4	15	24	51	5.98	
37	3.5	12	40	45	5.51	
38	15.6	11	37	36	4.49	A to ice edge
39	9.2	17	50	23	3.66	

near the ice edge where the mean ice draft decreases significantly while the percentage of thin ice becomes large. The values of $P'(h)$ for sections 1–10 were illustrated in Wadhams (1980).

To illustrate these changes more clearly, table 2 shows $P'(h)$ split into four depth bands: thin ice (less than 0.5 m draft); medium ice (0.5–2 m draft); 'undeformed' ice (2–5 m, a draft range which should include most of the level undeformed floes as well as some deformed ice); and 'ridged' ice (draft greater than 5 m). Data from sections 1–10 (Wadhams 1980) have been included to make the table complete. Percentages are rounded to the nearest whole number, except for thin ice.

Some conclusions that are apparent from this table are as follows.

(i) *Uniformity of ice in central Arctic.* Well away from the heavily ridged coastal zone off north Greenland the ice shows remarkably uniform characteristics. Sections 14–31 cover this central zone of the Trans-Polar Drift Stream, with 32 and 33 beginning to show slight coastal influence. A non-parametric run test (Bendat & Piersol 1971) was applied to each of the five parameters given in table 2, and sections 14–31 passed in every case. This indicates that each of the ice profiles is an independent sample of the same random variable, so that the entire 1800 km constitutes a homogeneous population. The mean value and range of variation for each parameter for sections 14–31, all data being uncorrected for beamwidth, are:

parameter	mean value	extreme 100 km limits	standard deviation
mean draft/m	5.37	4.69–6.02	0.06
0–0.5 m cover (%)	1.56	0.2–5.2	0.24
0.5–2 m cover (%)	6	4–10	0.5
2–5 m cover (%)	50	46–54	0.6
> 5 m cover (%)	42	36–48	0.7

The percentage of thin ice is relatively the most variable quantity from section to section. This exceptional uniformity was also found by Wadhams & Horne (1980) for ice in the central Beaufort Sea, although the mean ice draft was different.

(ii) *Abrupt edge to offshore ice zone.* The two most sudden transitions are between sections 13 and 14, and 33 and 34. That between 13 and 14 marks the change from the offshore north Greenland zone, with its heavy ridging, to less severe conditions of the central Arctic. The second transition, slightly less abrupt, marks the return of the submarine to the offshore zone further to the southeast. The first transition was investigated more closely by subdividing section 13 into four 25 km portions. The result is as follows, moving northward from section 13.1 to 13.4.

	percentage of ice (no beamwidth correction)				mean
section	< 0.5 m	0.5–2 m	2–5 m	> 5 m	draft/m
13.1	9	6	17	68	9.04
13.2	2	1	35	62	7.16
13.3	13	3	42	42	5.20
13.4	4	7	42	46	5.65

This demonstrates the extremely short length scale over which this major transition between ice régimes occurs. The main part of the transition appears to take place between portions 13.2 and 13.3, i.e. a length scale of about 25 km. This is a remarkable result, given that section 13 is already over 400 km from the coast of Ellesmere Island so that we are not dealing with

the familiar rapid transitions in ice characteristics that occur close to shore as in the Beaufort Sea shear zone (Reimnitz *et al.* 1977). Such a sudden transition far out at sea between a uniform mid-Arctic ice régime (sections 14–33) and a heavily ridged wide offshore régime (sections 1–12, 34–35) is a phenomenon that requires explanation in any theory of Arctic ice dynamics.

(iii) *Thin ice variability*. The thin-ice percentage varies greatly from section to section. The concentration of thin ice is generally low in the central Arctic (less than 2%), and high in the eastern part of the Greenland offshore zone (sections 2–5, 36–37) and close to the ice margin (sections 38–39). It is low in the western part of the Greenland offshore zone (sections 6–11) where heavy ridging does not coexist with plentiful thin ice, suggesting either that active ridge-building was not taking place or that ridging occurs there through shear or by crushing of thick ice blocks. The western Greenland offshore zone can be thought of as a shear zone for the Beaufort Gyre, while the eastern part is a shear zone for the Trans-Polar Drift Stream, so the difference in ice characteristics may reflect the differing origins and drift directions of the ice concerned.

(iv) *Downstream uniformity*. There is no significant progressive change in ice conditions with increasing downstream distance in the Trans-Polar Drift Stream. The axis of the Arctic mid-Oceanic Ridge roughly corresponds with the mean direction of ice drift, so that the six Ridge transects represent samples of ice conditions at increasing downstream distance. The third transect shows an increase in mean draft, but there is no obvious trend from the first to the sixth.

(v) *Temporal variations in Fram Strait*. There are considerable differences between the ice thickness distributions in sections 1, 2 and 3 and those in 37, 36 and 35 which correspond except for being 15 km nearer the coast and obtained 11 days later. The mean draft is lower in the later set (except for 35) and there is more thin and young ice. Ice charts often show a semi-permanent winter polynya lying off the mouth of Danmarks Fjord, and section 4 on the outward track shows an unusually large amount of thin ice. It appears that the limits of this 'polynya' (or area of reduced ice concentration) have changed between the outward and homeward legs, so that it is sampled further to the southeast during the later transect.

(vi) *Approach to ice margin*. Section 39 was examined by subdivision to investigate the change in ice conditions near the ice margin. The subdivisions were 25 km long (39.1–39.4), with a final 35 km portion (39.5) which terminates at the ice edge itself. The results are as follows:

	percentage of ice (no beamwidth correction)				mean
section	< 0.5 m	0.5–2 m	0.5–2 m	> 5 m	draft/m
39.1	8	16	43	34	4.63
39.2	7	16	47	31	4.24
39.3	16	20	44	20	3.15
39.4	11	15	51	23	3.50
39.5	5	19	64	12	3.06

The decline in mean draft as the edge is approached can be seen as being mainly due to the decline in the fraction of deformed ice (draft > 5 m). Thus one of the chief characteristics of marginal zone ice is the scarcity of ridges, in agreement with the results from the Denmark Strait of Kozo & Diachok (1973), Kozo & Tucker (1974) and Westhall & Li (1976), who found no keels deeper than 6.1 m until 94 km inside the ice edge.

So far we have dealt with uncorrected data. We now wish to compare our results with those

of other observers, so it is necessary to apply a beamwidth correction to the ice drafts. Figure 7 shows the result of applying the wide-beam simulation technique to the *Gurnard* data, testing for mean draft. It can be seen that the draft transformation is linear, and the narrow-beam mean draft $\bar{h}_n$ is related to the wide-beam mean draft $\bar{h}_w$ by

$$\bar{h}_n = 0.840\bar{h}_w. \tag{6}$$

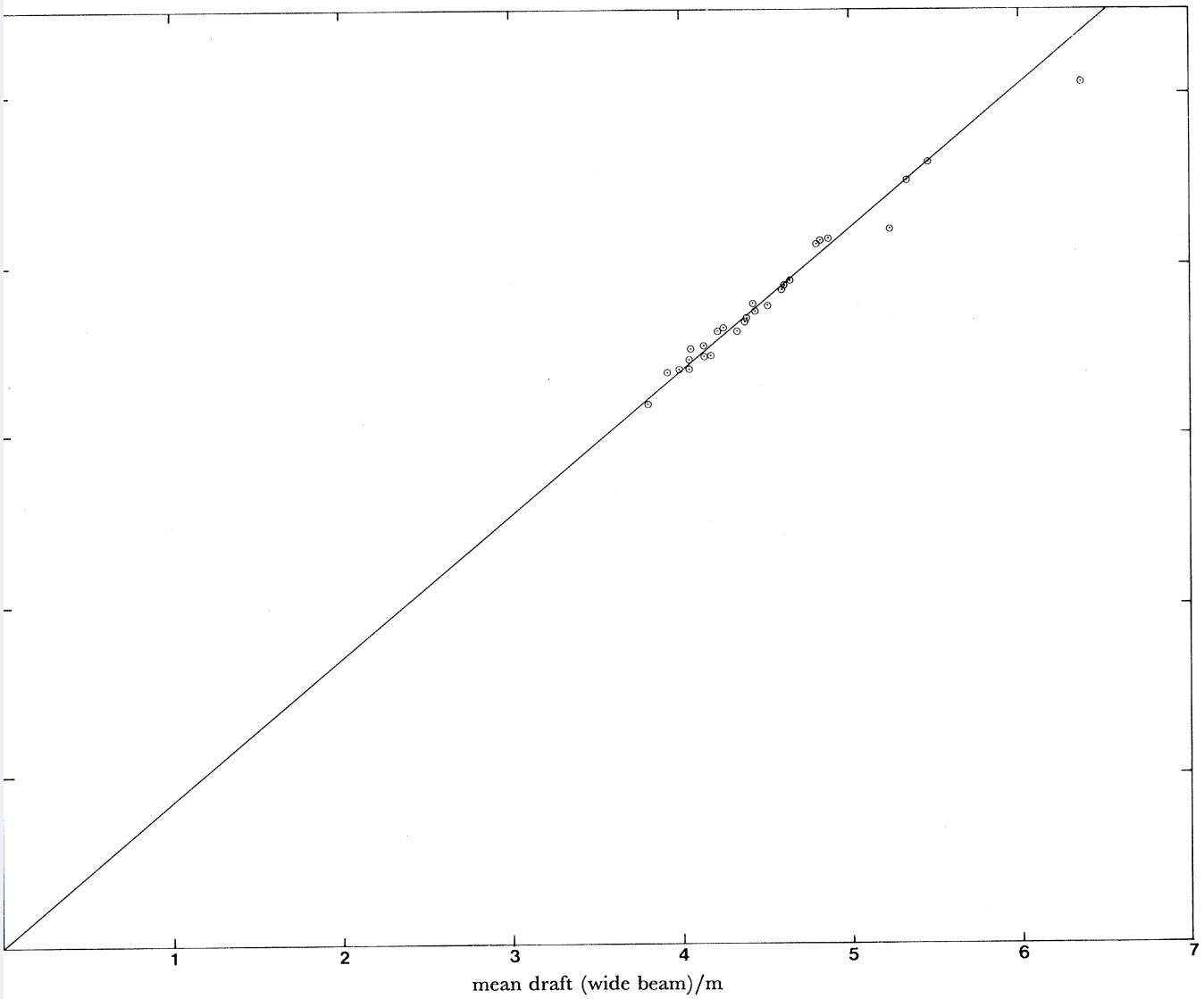

FIGURE 7. Result of applying a simulated wide beam to 50 km sections of the *Gurnard* profile: effect on mean draft of section.

This is from a least squares fit forced to pass through the origin, and the result must be interpreted with caution as it is only really valid over the range $3.2 \leqslant \bar{h}_n \leqslant 4.7$ m (the single point at $\bar{h}_n = 5.1$ m lies off the line). Application of the result – a simple 16% draft reduction – to deeper mean drafts may not be valid. Direct application of deconvolution to the *Sovereign* data produced an average draft reduction of only 9%, making it clear that deconvolution

does not restore the original profile adequately, and that the statistical simulation technique is preferable. Deconvolution was therefore used only where absolutely necessary to supplement the results of simulation.

The conversion of the percentages in each of the categories of table 2 involved a greater degree of scatter, as is shown in figure 8. The 2–5 m and above 5 m ranges give results that can be fitted well by a straight line, while the 0.5–2 m range can be fitted by a smooth curve. The 0–0.5 m range does not give good results, because the maximum percentage of thin ice observed in a *Gurnard* section was only 3.5, yielding 2% when transformed to wide beam. The line of best fit is therefore valid only up to 2% of apparent thin ice. In table 2 the percentages go up to 15.6, and these had to be corrected by direct application of deconvolution, which is of dubious accuracy.

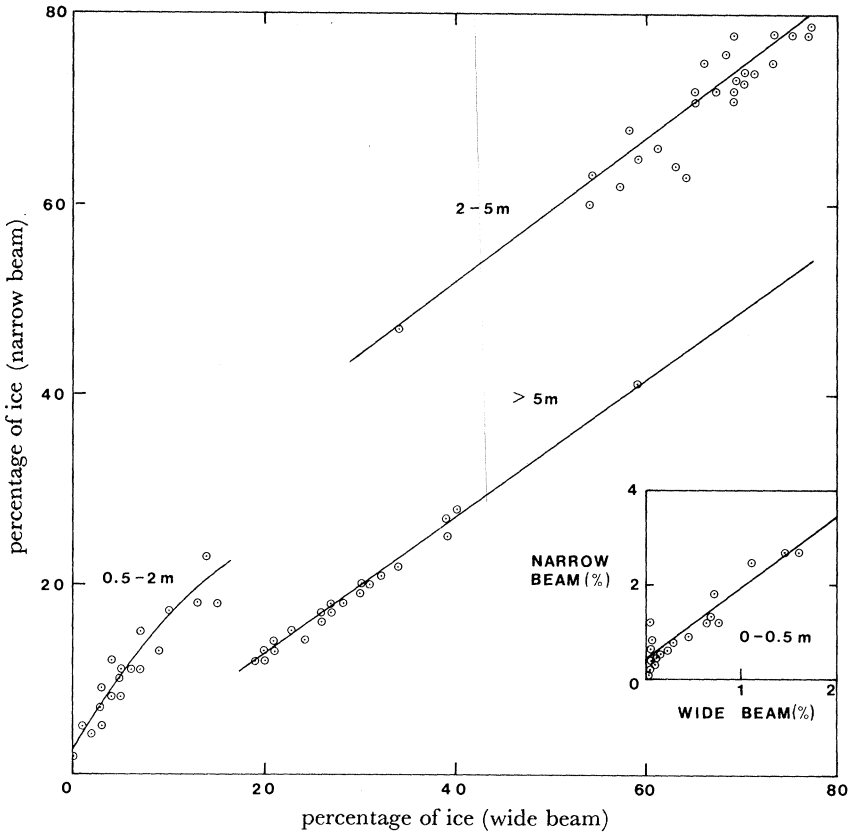

FIGURE 8. Result of applying a simulated wide beam to 50 km sections of the *Gurnard* profile: effect on percentages of ice in four draft categories.

Table 3 is the final result of correcting table 2 for beamwidth effects, by using the results of figures 7 and 8 where possible and renormalizing when the total percentage generated thereby differed from 100. Absolute accuracy cannot be guaranteed, but we feel that the results are subject to random rather than systematic errors and that table 3 is as reliable a final product as can be obtained.

The data from table 3 can now be compared with corresponding data from the *Dreadnought* and *Gurnard* cruises. The *Dreadnought* profile (Swithinbank 1972; Williams *et al.* 1975) covered

a 560 km track from 85° to 90° N along 6° to 7° E, which corresponds most closely to sections 17–21 of the *Sovereign* data. The comparison is as follows.

profile	percentage of ice < 0.5 m	0.5–2 m	2–5 m	> 5 m	mean draft/m
Dreadnought					
wide beam deconvolved	2.7	9	55	33	4.59†
Sovereign, 17–21					
wide beam uncorrected	1.9	5	52	41	5.28
corrected by simulation	2.9	10	59	27	4.44
deconvolved	2.0	6	56	36	4.87

† Corrected from the figure of 4.29 misprinted in Williams *et al.* (1975).

The figures that are directly comparable are those from *Dreadnought* and *Sovereign* corrected by deconvolution, since this was the technique applied to the *Dreadnought* data before generation

TABLE 3. ICE DRAFT DISTRIBUTION: PERCENTAGES IN DIFFERENT DRAFT BANDS, CORRECTED FOR BEAMWIDTH EFFECT

section	percentage of ice < 0.5 m	0.5–2 m	2–5 m	> 5 m	mean draft/m
1	3.2	9	42	45	5.84
2	10.0	10	40	40	5.77
3	9.4	10	39	42	5.78
4	13.4	13	38	35	5.07
5	10.1	11	44	36	5.38
6	3.3	6	43	47	6.66
7	3.6	4	47	46	6.32
8	2.1	6	46	46	6.31
9	3.7	5	48	44	6.05
10	2.5	4	38	55	7.49
11	2.6	5	51	42	6.14
12	5.1	5	49	40	6.41
13	8.3	9	46	37	5.72
14	4.3	9	62	25	4.38
15	1.0	16	55	28	4.44
16	2.5	15	56	26	4.25
17	6.4	15	56	23	3.94
18	2.6	9	61	27	4.41
19	2.4	9	59	30	4.60
20	2.0	10	59	29	4.64
21	1.3	9	62	28	4.60
22	4.2	11	60	25	4.50
23	3.1	14	58	25	4.23
24	2.6	11	58	29	4.59
25	2.6	10	56	31	4.94
26	2.1	10	55	33	5.06
27	2.3	13	59	26	4.35
28	0.5	10	59	31	4.67
29	2.1	11	59	28	4.46
30	1.3	9	62	28	4.51
31	3.3	12	56	28	4.55
32	6.3	9	52	33	4.86
33	9.6	17	44	30	4.80
34	2.6	11	43	43	5.97
35	2.1	14	41	43	6.35
36	11.2	20	37	32	5.02
37	4.7	17	49	29	4.63
38	16.3	16	45	22	3.77
39	10.1	21	55	14	3.07

of statistics. The results show an increase of mean draft of 0.28 m between March 1971 and October 1976. This is probably an underestimate because *Dreadnought's* sonar beam was wide in two planes while the deconvolution was applied in only one plane. Our confidence that this is a real effect is increased by the data acquired by U.S.S. *Nautilus* in August 1958 within the latitude range 90–85° N at 25° E (Lyon 1961; interpreted by Williams *et al.* 1975). *Nautilus* had a sounder with 12° beamwidth, and the uncorrected data gave a mean draft of 5.56 m, slightly greater than *Sovereign's* uncorrected results. We conclude, therefore, that the mean draft of ice in the Eurasian Basin in late summer (August–October) is greater, by at least 0.3 m, than the mean draft in March. An explanation for this, suggested by Williams *et al.* (1975), is that in winter the ice profile is dominated by large stretches of young and first-year ice which bias $P(h)$ towards a lower mean value despite the fact that multi-year ice is thicker in winter than in summer.

A comparison of the homogeneous part of the *Sovereign* profile (sections 14–31) with the homogeneous portion of the *Gurnard* profile (Wadhams & Horne (1980), sections 3–25 which lie in the southern Beaufort Sea beyond the offshore zone) yields the following results:

	percentage of ice				
profile	< 0.5 m	0.5–2 m	2–5 m	> 5 m	mean draft/m
Sovereign central Eurasian Basin, corrected by simulation	2.6	11	58	28	4.51
Gurnard central Beaufort Sea, narrow-beam profile	1.0	10	72	17	3.67

The *Gurnard* profile was acquired in April 1976. The seasonal effect can be expected to be in the same direction as the *Sovereign–Dreadnought* comparison, but the difference in this case – 0.84 m – is great enough to indicate a geographical effect as well. The picture of the central Arctic Ocean which this suggests is of ice characteristics that are statistically homogeneous on length scales of about 1000 km but that vary slowly across the Arctic Basin so that the mean draft of ice on the European side is greater than the mean draft in the Beaufort Sea. This is in agreement with an analysis by LeSchack & Chang (1977; reproduced as figure 18 of Hibler 1979) of short profile lengths from U.S. submarine cruises of 1960–62, which yielded a tentative contour map of mean drafts in the Canada Basin; the drafts increased steadily from a Siberia–Alaska axis across towards north Greenland.

Table 3 also shows that the offshore zone of north and northeast Greenland (sections 1–13, 34–35) displays mean drafts (5.3–7.5 m) that are far higher than the highest mean draft found in the offshore zone of the Beaufort Sea (5.09 m in *Gurnard*, section 1, Wadhams & Horne (1980)). This confirms that the north Greenland–Ellesmere Island ice zone is a more formidable region of ice build-up than the Alaskan offshore region, and probably represents the heaviest ice conditions in the Arctic Ocean (and hence the world). Nothing in the Antarctic can match such deformation, and the only possible competitor is the offshore zone from Axel Heiberg Island to Prince Patrick Island, where unclassified sonar profiles have not yet been obtained.

Finally we consider the analytical form taken by the ice draft distribution at great depths. Wadhams & Horne (1980) found that the ice draft distribution from the narrow-beam *Gurnard* data fitted a negative exponential at drafts beyond 6 m. They also found that the distribution of keel drafts fitted a negative exponential, and were therefore able to tie the two results together by supposing that at drafts beyond 6 m all ice is necessarily deformed and therefore

PHILOSOPHICAL TRANSACTIONS OF THE ROYAL SOCIETY A MATHEMATICAL, PHYSICAL & ENGINEERING SCIENCES

exists on the flanks or bottoms of pressure ridges. If ridges are assumed to take an average shape consisting of isosceles triangles of uniform slope angle, then the keel and ice draft distributions will have the same analytical form. Figure 9 shows semilogarithmic plots of *Sovereign* ice draft distributions, uncorrected for beamwidth effects. Two curves are illustrated: one is the overall distribution for sections 11–39, covering mainly the central Arctic régime, and the other is section 11, typical of the north Greenland offshore zone. Both distributions fit a negative exponential at drafts beyond 8–10 m, the section in heavily deformed ice having a lower gradient than the distribution covering less severe ice conditions.

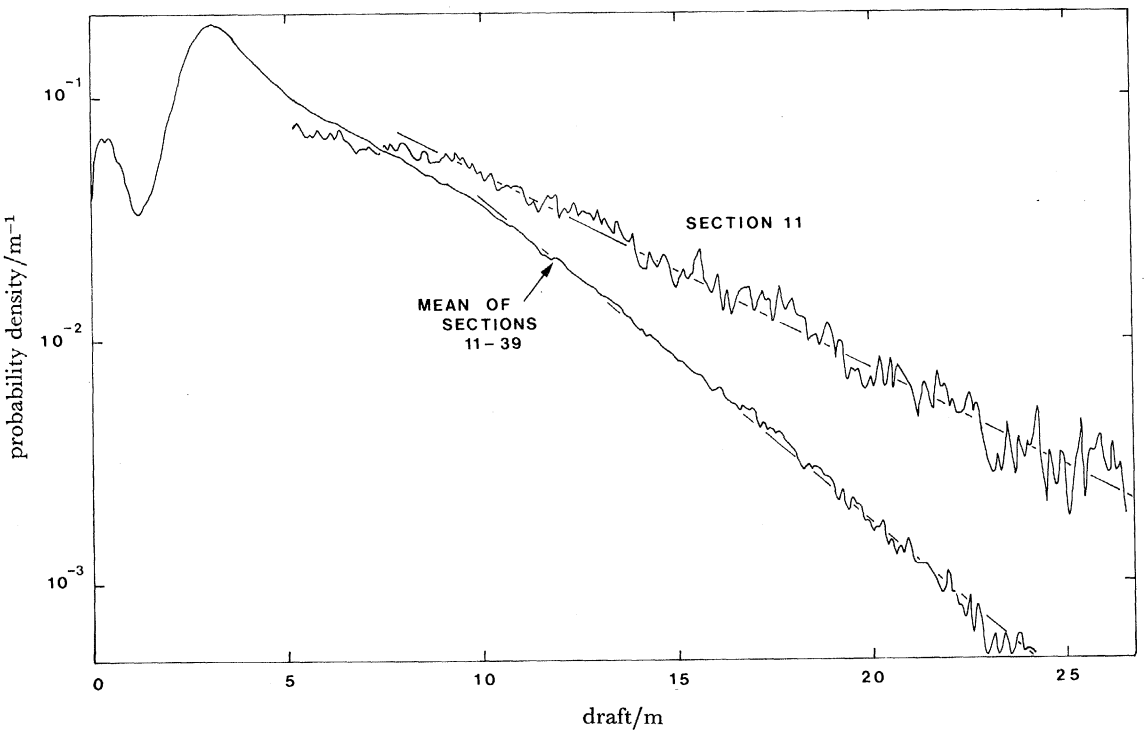

FIGURE 9. The fit of the ice draft distribution to a negative exponential at large depths. $P'(h)$ is plotted in 10 cm depth increments on a semilogarithmic scale, for section 11 and sections 11–39 respectively.

Elevation

Table 4 shows the distribution of ice elevation derived from the laser profiles. The elevation is relative to a zero datum corresponding to the mean freeboard of undeformed floes. Elevation distributions for sections 1–10 were illustrated in Wadhams (1980), demonstrating the sharp single peak close to zero elevation.

Resemblances between table 4 and table 3 are easy to spot. The mean elevation over the Greenland offshore zone is very high, and there is a sharp drop at section 13, both in mean elevation and in the percentage of highly deformed ice (elevation more than 1 m). However, because of the variable zero datum that had to be used in processing, the values in table 4 must be treated with caution. Ice in the first category (elevation less than zero) consists mainly, although not entirely, of ice in leads and polynyas, and we therefore expect its occurrence to be positively correlated with the percentage of thin ice in the sonar profile. Most of the undeformed ice falls into the 0–0.5 m bin, and its occurrence should be positively correlated

with the percentage of ice in the 2–5 m draft category. The ice of elevation greater than 1 m must be contained in pressure ridge sails; this should be positively correlated with ice deeper than 5 m in the sonar statistics. Lastly, we hope that the mean elevation is positively correlated with the mean ice draft.

TABLE 4. ICE ELEVATION DISTRIBUTION FROM LASER PROFILES

	percentage of ice				mean elevation
section	< 0 m	0–0.5 m	0.5–1 m	> 1 m	m
1	24	60	11	5	0.229
2	27	54	13	6	0.244
3	27	51	15	7	0.269
4	31	49	13	7	0.247
5	19	57	16	8	0.336
6	8	55	23	14	0.492
7	17	55	18	9	0.375
8	12	55	21	12	0.445
9	11	61	19	9	0.399
10	17	54	19	10	0.389
11	15	65	14	6	0.294
12	15	62	14	9	0.336
13	12	68	14	6	0.309
14	13	72	11	4	0.248
15	16	70	11	4	0.244
16	22	62	13	4	0.223
17	23	63	11	4	0.211
18	18	69	9	3	0.205
19	34	57	7	3	0.140
20	27	60	10	3	0.190
21	28	57	10	5	0.212

Figure 10 shows the mean elevation $\bar{h}_t$ plotted against mean draft $\bar{h}_d$. There is considerable scatter, but the straight line of best fit is

$$\bar{h}_d = 8.35\bar{h}_t + 3.04 \tag{7}$$

with a correlation coefficient of 0.79. If the top and bottom tracks were perfectly correlated, the intercept at $\bar{h}_t = 0$ would represent the mean draft of undeformed ice floes (3.04 m) while the gradient would represent the ratio of added draft to added elevation, which is $(\rho_i)_{sails}/[\rho_w - (\rho_i)_{keels}]$. Here, $(\rho_i)_{sails}$ and $(\rho_i)_{keels}$ are the mean densities of ice added to sails and keels respectively. As a check, if we assume that $(\rho_i)_{sails} = (\rho_i)_{keels} = \rho_i$, then (7) would give $\rho_i = 0.915$. Both this and the intercept to (7) are reasonable values. Therefore (7) can be used as a tool for predicting the mean draft of a polar icefield from the results of a laser-profiling survey over it, which is of value since laser profilometers are more readily available for routine surveys than submarines.

The other correlations suggested above were tested with the following results for linear regression and correlation coefficient:

		$(y = a_1 x + a_0)$		correlation
x	y	a_1	a_0	coefficient
> 1 m elevation (laser) (%)	> 5 m draft (sonar) (%)	2.33	21.4	+0.79
0–0.5 m elevation (laser) (%)	2–5 m draft (sonar) (%)	0.840	−0.684	+0.64
< 0 m elevation (laser) (%)	< 0.5 m draft (sonar) (%)	0.129	2.20	+0.27

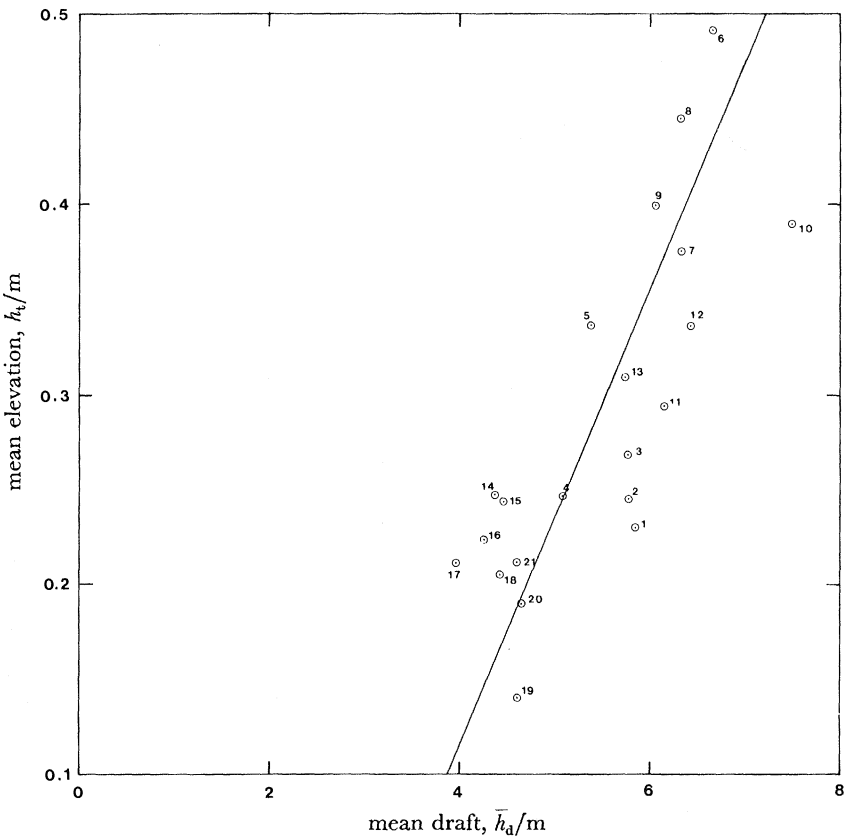

FIGURE 10. Mean elevation of ice in 100 km laser profile sections plotted against mean draft in corresponding sonar section.

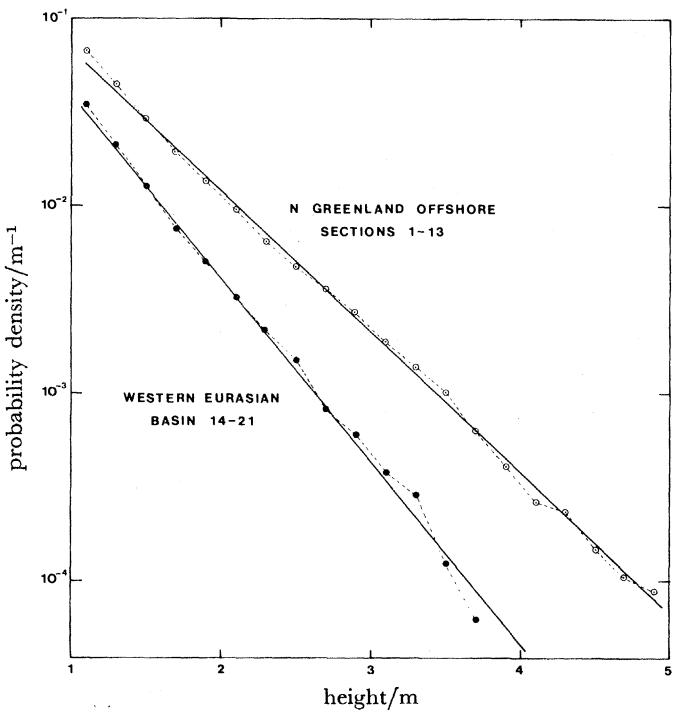

FIGURE 11. Fit of ice elevation distribution to a negative exponential at heights beyond 1 m. $P(h)$ is plotted in 20 cm height increments on a semilogarithmic scale, for sections 1–13 and 14–21 respectively.

The best correlation is between the percentages of ice with high elevation (above 1 m) and draft (below 5 m), the percentages of 'undeformed' ice (0–0.5 m elevation, 2–5 m draft) also being well correlated. The correlation between high elevation and draft suggests that, if we assume a 1:1 correspondence between keel and sail numbers, the creation of a keel–sail pair involves the addition of 2.33 as much width to the keel baseline at the 5 m level as it does to the sail baseline at the 1 m level. This, of course, is the familiar result that the keel of a ridge is much wider than its sail.

The form of the ice elevation distribution at great heights is shown in figure 11, where the overall results for the Greenland offshore zone (sections 1–13) and the western Eurasian Basin (sections 14–21) at elevations beyond 1 m are plotted in 20 cm bins on a semilogarithmic scale. At this height above the mean level ice surface all contributions to the probability density function (p.d.f.) must come from ice in deformation structures such as pressure ridges. As in the case of draft, there is a good fit to a negative exponential distribution, but with a small systematic deviation from a perfect fit. Again the offshore zone possesses more deformed ice than the central Arctic régime, and the p.d.f. falls off more slowly with increasing height.

Level ice

Both casual observation and fabric analysis of ice-fields tell us that the surface area of an ice-covered sea is made up of two distinct categories of ice: 'undeformed' ice, that is, ice that has reached its present thickness by natural thermodynamic growth alone (including open water and young ice in polynyas); and 'deformed' ice, which has reached its present disposition by mechanical processes (pressure and shear ridges, hummocks, rafted ice). Therefore, despite recent suggestions that the whole topography of an ice cover be dealt with as a single statistical process (Rothrock & Thorndike 1980), it seems physically reasonable to base theoretical models on the idea that it is the sum of one or more types of undeformed ice (young, first-year, multi-year) and of deformed ice which is composed of entities called 'ridges'. We first consider undeformed ice.

The function $P(h)$, while revealing much about the nature of the ice cover, does not unequivocally discriminate between deformed and undeformed ice, neither does it efficiently define the preferred drafts of undeformed floes. To attempt such a discrimination we need to pick out a characteristic property of undeformed ice, and the most obvious one is its comparative flatness. By trial and error Williams *et al.* (1975) found that if 'level ice' were defined as ice with a local gradient of less than 1 in 40, then statistically generated level ice percentages agreed well with the results of visual estimates of undeformed ice. The precise way in which the 'local gradient' is defined has been a matter of controversy (Wadhams & Horne 1980); one particularly restrictive definition has the effect of very efficiently delineating preferred drafts but generating very little 'level ice'. In this paper we shall use the definition adopted by Wadhams & Horne (1980; their D1) for the sake of uniformity; this states that a 'level ice point' is one whose draft differs from that of a point 10 m to either side by less than 25 cm. This allows a certain contribution from fortuitously spaced pressure ridges, but results in percentages that agree with visual estimates to within $\pm 10\%$.

Figure 12 shows the distribution of level ice draft averaged over sections 11–39. The shape of the curve is similar to that of most individual 100 km sections, i.e. a *single* major peak at about 3 m draft with a minor peak for thin ice. By contrast, the distributions found by Wadhams

& Horne for the Beaufort Sea possessed two or more major peaks. Wadhams & Horne's averaged distribution possessed two clearly separated peaks, the first at 2.0–2.2 m draft and the second, broader peak at 2.7–3.1 m draft. The explanation suggested by Wadhams & Horne was that the 2.0–2.2 m peak represents first-year ice and the second peak (which in some sections was further bifurcated into one at 2.7–2.8 m and one at 3.1–3.2 m) represents second- and multi-year ice. This suggestion finds support in the present results, since in October there

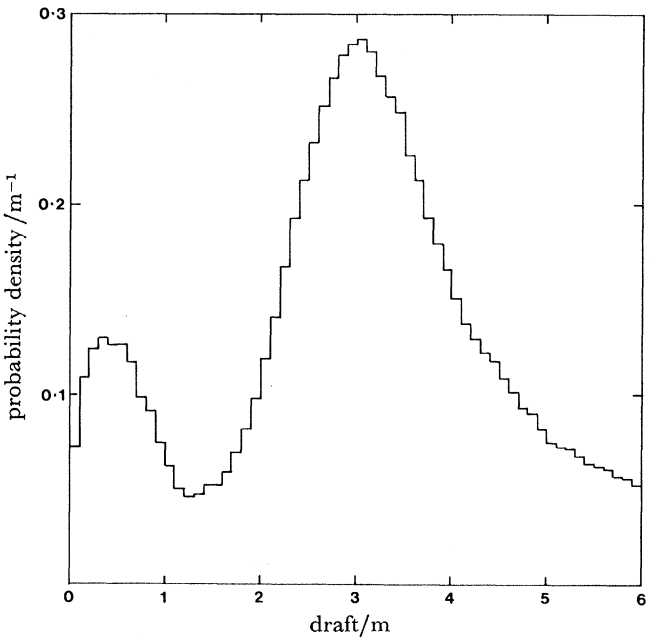

FIGURE 12. Distribution of level ice draft in the range 0–6 m, averaged over sections 11–39, obtained by using uncorrected sonar data.

has not been sufficient time for any first-year ice to grow, so that we expect all 'level ice' to be either young ice (less than 1 m thick), or second-year ice or older. The conclusion is that the peak of the curve – at 3.0–3.1 m – is the preferred draft reached in early winter by second- or multi-year ice which has grown thermodynamically. The thickness implied by this, 3.3–3.5 m, is greater than that predicted in Thorndike *et al.* (1975) and by Maykut & Untersteiner (1971), who predicted 2.7 m as the thickness reached by an ice cover in thermodynamic equilibrium in late October. It agrees, however, with equation (7). The young ice peak in figure 12 lies in the range 30–60 cm, in agreement with the mean ice thickness found in polynyas during surfacings (41 ± 7 cm, measured during seven surfacings).

We expect the percentage of the profile occupied by level ice to vary inversely with the mean ice draft, and this is seen in figure 13, where the section numbers are also given to illustrate the range of variation. In the Greenland offshore zone the percentage of level ice varies from 28 to 43, while in the marginal ice zone it approaches 60. Figure 13 also distinguishes the different régimes of ice cover very clearly. Sections 1–10 fall within a clearly defined trend, while the central Arctic sections fall within the same small area. Sections 11–13 and 34–35 constitute an 'outer offshore zone' where the mean draft is as high as in the inner offshore zone but where the fraction of level ice is greater, presaging the transition to the central Arctic régime.

A similar relation holds for laser data, as shown in figure 14, with similar relative positions of the diagram for the different ice régimes. The absolute percentage of level ice is higher, since the sails of ridges are narrower than their keels. If we assume that all ice that is not 'level ice' is deformed ice, then comparison of figures 13 and 14 shows that in the central Arctic régime the percentages of deformed ice are 9–14 on the surface and 46–56 on the

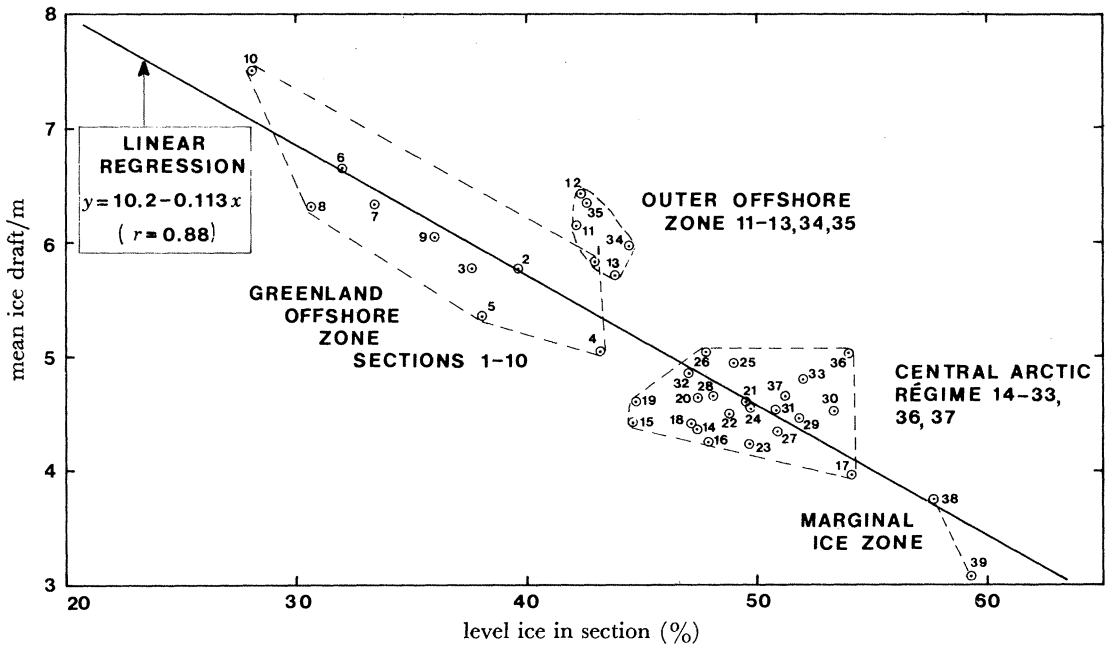

FIGURE 13. Percentage of level ice in a sonar section plotted against mean draft of section corrected for beamwidth.

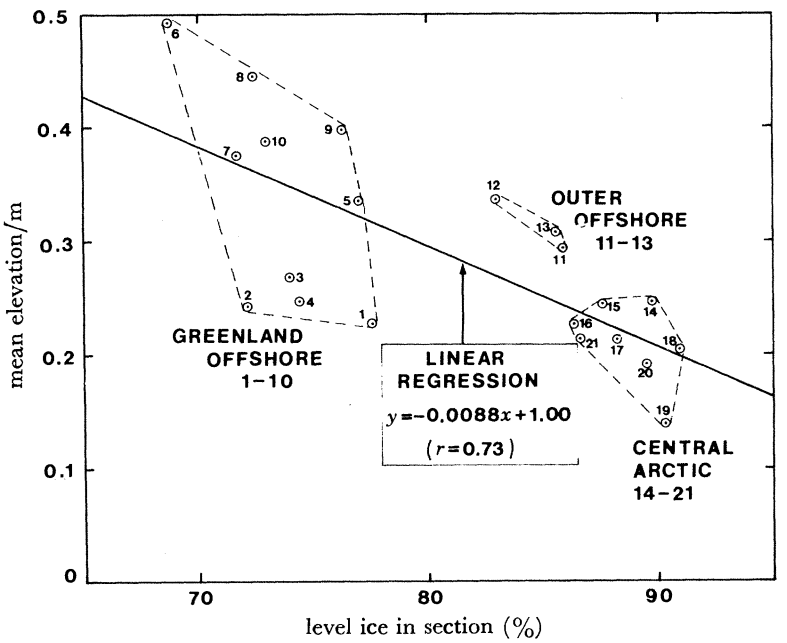

FIGURE 14. Percentage of level ice in a laser section plotted against mean elevation of section.

bottom, a ratio of 1:4 or 1:5. In the Greenland offshore zone, however, the percentages are 22–32 for the surface and 57–72 for the bottom, a ratio of 1:2.3–1:2.6. This can be explained by supposing that under moderate deformation the pressure ridge keels are well separated. Then, as the ridging intensity increases the keels begin to overlap while the sails remain as distinct entities. The effect of overlap on keel distributions is explored in the next section, and in Lowry & Wadhams (1979).

Distribution of ridge spacings

Definition of a ridge

The entity that we shall define as a 'ridge' must be to some extent a statistical artefact, since in a one-dimensional ice profile it is impossible to identify the form and origin of every topographic feature. Nevertheless we hope that the mathematical entity that we construct bears a reasonably close resemblance to those definite features which an aerial observer recognizes as pressure and shear ridges. We shall define an *independent ridge* as a deformed ice feature in which the point of maximum draft or elevation (the crest) is bracketed by points (the troughs) whose vertical distance from the datum of local undeformed ice is less than half that of the crest. This is analogous to the Rayleigh criterion for separating spectral lines, and has been used as the ridge definition in analyses by Lowry & Wadhams (1979), Tucker *et al.* (1979), Wadhams (1976, 1978*a*, 1980), Wadhams & Horne (1980), Wadhams & Lowry (1977), Weeks *et al.* (1980) and Williams *et al.* (1975). The only difficulty in the definition is that of locating the datum of local undeformed ice. For a laser profile processed as described in this paper it is simply the zero datum, and the elevation of the ridge sail crest is just its height above zero (so that the elevation of a sail which is sandwiched between a floe and a lead is its elevation above the floe surface). For a submarine profile the location of the datum would require the use of a time-consuming algorithm, so for simplicity we define the datum arbitrarily as 2.5 m draft (see also Wadhams & Horne 1980). A ridge keel of draft h at the crest therefore has troughs of draft less than $\frac{1}{2}(h-2.5)$. The true keel relief (equivalent of the sail elevation) is unknown but is assumed to be given by $h-2.5$.

The spacings of keels

Hibler *et al.* (1972) showed that if pressure ridges occur at random in an ice profile, the probability density $P_r(x)$ of spacings x between ridges is given by

$$P_r(x) = \mu \exp(-\mu x)\,\mathrm{d}x, \tag{8}$$

where μ is the mean number of ridges per unit length of profile track. Mock *et al.* (1972) found that ridges identified from aerial photographs fitted this relation well. More recently, Lowry & Wadhams (1979) derived a modified relation which allows for the possibility of ridges overlapping so that the trough between two crests disappears. The shallower of the two closely spaced ridges is thus lost from the statistics. This is the so-called 'ridge-shadowing effect'. If two ridges have reliefs h, h' ($h > h'$) and are assumed to be triangular in cross section with slope α in the along-track direction, then the closest approach x_{crit} of the two ridges that still permits h' to be independent is

$$x_{\mathrm{crit}} = h \cot \alpha. \tag{9}$$

The relation based on this idea was found to give better agreement with ice profile data at small spacings.

Figure 15 shows the overall distribution of spacings for keels of draft greater than 5 m and 9 m. Keel statistics have to be quoted relative to a low-value cut-off, since there is a range of drafts where it is impossible to distinguish between a keel and a natural undulation of a floe bottom; the cut-off should be chosen so as to exclude drafts where undeformed floes can contribute to the count of 'keels', i.e. at about 5 m. It can be seen that the spacing distribution fits a negative exponential at spacings above 140 m, but that there is a deficit of keels at closer

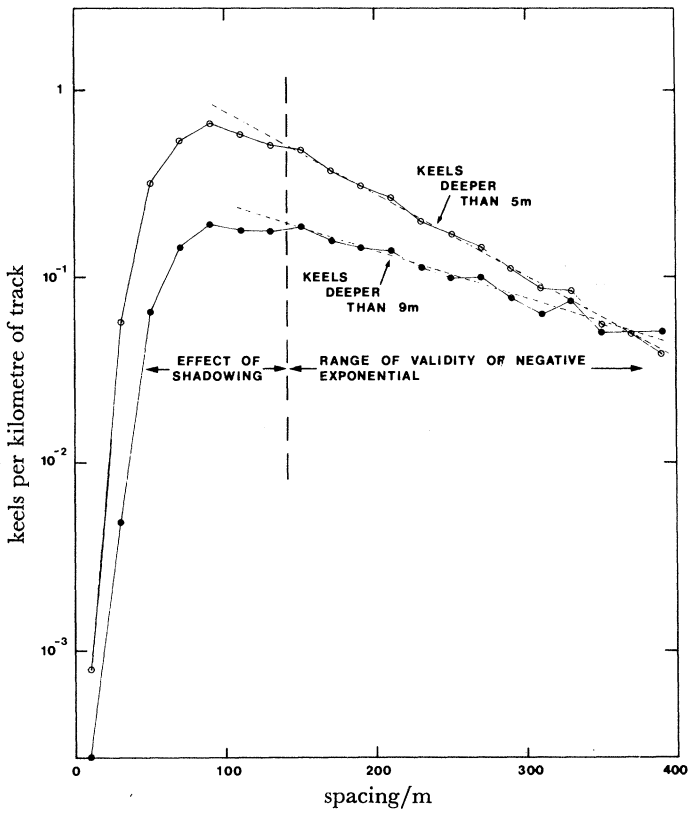

FIGURE 15. Overall distribution of keel spacings from entire sonar profile, for keels of draft greater than 5 m and 9 m, in 20 m spacing bins.

spacings. A similar effect was found by Wadhams (1980) in an analysis of the first ten sections, while Wadhams & Horne (1980) found that the shadowing effect extended only to 40 m spacing for a narrow-beam sonar profile. The magnitude of the keel-shadowing effect is therefore a function not only of the degree of ridging but also of the transducer beamwidth. A wide-beam sonar makes keels appear to have a shallower slope than they really possess (Wadhams 1978*a*) and conceals troughs between close crests. The result, as found by Lowry & Wadhams (1979), is that a modified theory must use a very low value for equivalent slope angle α to fit the data.

The gradients of the exponential portions of figure 15 were used to predict μ from (8); the resulting ratios of predicted μ to measured μ were 2.02 for 5 m cut-off and 1.38 for 9 m cut-off. If indeed ridges are purely randomly spaced down to the smallest spacings, then the true

PHILOSOPHICAL TRANSACTIONS OF THE ROYAL SOCIETY A MATHEMATICAL, PHYSICAL & ENGINEERING SCIENCES

number of keels per kilometre with 9 m draft or more is 38% greater than the number found by our statistics, and the number deeper than 5 m is 102% greater.

The spacings of sails

Figure 16 shows the overall distribution of sail spacings, for sails of elevation greater than 60 cm and 1 m. The shadowing effect is now seen only in the first bin (0–20 m spacing), partly because sails are built on much narrower bases than keels and therefore overlap less frequently, and partly because a laser has an extremely narrow beamwidth. A negative exponential gives an approximate fit to the data for moderate spacings, but there is an excess of

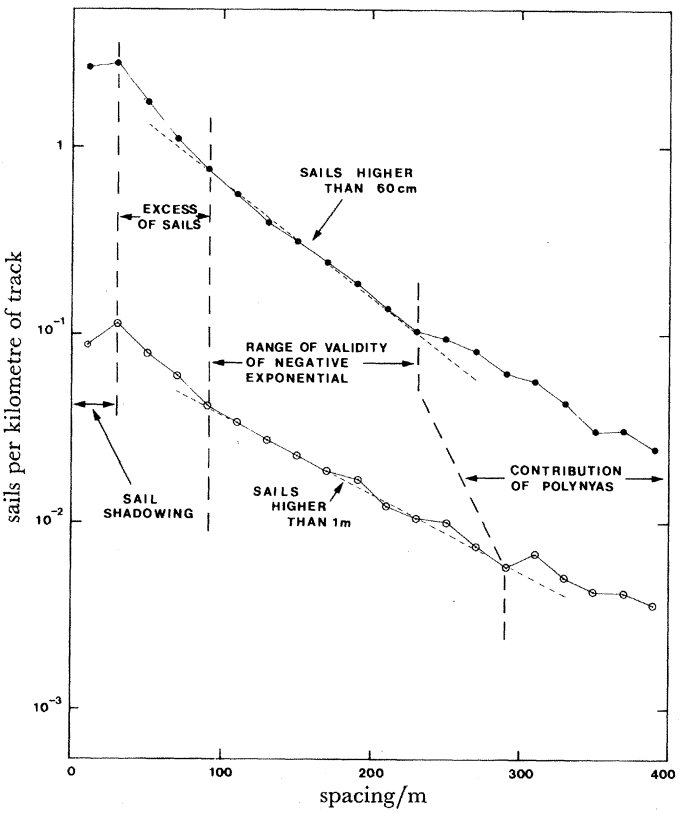

FIGURE 16. Overall distribution of sail spacings from entire laser profile, for sails of elevation greater than 60 cm and 1 m, in 20 m spacing bins.

sails in the 20–80 m spacing range and at very large spacings. The excess at large spacings can be explained by the presence of leads and polynyas, which interpose smooth stretches of ice into a previously random icefield and thus generate an anomalous number of large sail spacings; such an effect was also seen in Beaufort Sea keels (Wadhams & Horne 1980). An excess of 20–80 m spacings was also seen by Mock *et al.* (1972) in sails counted from aerial photographs. A possible explanation lies in the mechanics of ridge building, which allow a single well defined keel (smoothed by water-flow and erosion) to possess a complex and irregular sail which may be perceived by the computer as being composed of closely spaced entities. This results in both an excess of closely spaced sails and in a greater number of sails than keels being counted in the same icefield. Ackley *et al.* (1974), for instance, found that a conversion

from top to bottom surface relief could be accomplished quite reliably by isostatic compensation accompanied by a filter that smoothes out bottom surface irregularities relative to those of the top surface.

Distribution of ridge elevations and drafts

Theory and previous observations

Hibler, Weeks & Mock (1972, henceforth H.W.M.) derived a theoretical distribution of ridge heights by assuming that ridges are randomly oriented linear features which are geometrically congruent in cross section, i.e. have a cross-sectional area proportional to the square of their relief (depth or height relative to local level-ice surface). A variational calculation then yields the most likely distribution of ridge heights that will produce a given volume of deformed ice per unit area of icefield. The result is

$$P_r(h)\,\mathrm{d}h = 2\lambda\bar{h}\exp(\lambda h_0^2)\exp(-\lambda h^2)\,\mathrm{d}h, \tag{10}$$

where $P_r(h)$ is the probability that the relief lies between h and $h+\mathrm{d}h$; $\bar{h}$ is the mean relief; h_0 is a low value cut-off; and λ is a parameter to be derived by iteration from

$$\exp(-\lambda h_0^2) = h(\lambda\pi)^{\frac{1}{2}}\,\mathrm{erfc}\,(\lambda^{\frac{1}{2}}h_0). \tag{11}$$

Lowry & Wadhams (1979) have shown how (10) is modified by the ridge shadowing effect; the modification is minor and causes a small deficit of ridges at the low height end of the distribution. H.W.M. and Hibler *et al.* (1974) fitted (10) to a wide range of sonar and laser data; it was also found to fit sonar data from H.M.S. *Dreadnought* (Lowry & Wadhams 1979) and sonar data from the first ten sections of the *Sovereign* track (Wadhams 1980).

An alternative empirical distribution has the more simple form

$$P_r(h)\,\mathrm{d}h = B\exp(-bh)\,\mathrm{d}h, \tag{12}$$

where

$$B = b\exp(bh_0) \tag{13}$$

and

$$b = (\bar{h}-h_0)^{-1}. \tag{14}$$

In this case h can be chosen to be ridge relief or actual draft/elevation relative to sea level; the form of the distribution is unaltered and only the constants are modified. Equation (12) was found to fit narrow-beam sonar data from the *Gurnard* cruise (Wadhams & Horne 1980), as well as laser profiles that were analysed by using the Rayleigh criterion (Wadhams 1976, 1980; Tucker *et al.* 1979; Weeks *et al.* 1980; Leppäranta 1981).

The implication is that (10) holds only for data from wide-beam transducers, while the greater resolution of ridge structure attained by a narrow-beam instrument shifts the distribution to the more random law of (12). This suggests that the H.W.M. analysis may be valid for deformation elements each of which is the result of a single lead closure, i.e. a single ridge-building event. Such an element is smoothed out by a wide beam transducer and perceived as being a single ridge. A narrow beam transducer, however, probes into its complex structure and picks out peaks and troughs; the distribution of ridge heights then resembles the distribution of ice draft or elevation itself. We have already seen that the thick end of the ice draft/elevation distribution is a negative exponential. Therefore the problem of finding the physical basis for the empirical distribution (12) is transformed into the problem of finding the physical

reason for the ice draft distribution being a negative exponential at its thick end; this can only come trom a much closer examination of the mechanics of ice deformation.

The distribution of keel drafts

Figure 17 shows the overall distribution of keel drafts from the entire record, plotted on a semilogarithmic scale of keel frequency against $(h-2.5)^2$, where h is the keel draft and $h-2.5$ the presumed keel relief. There is a good fit to (10) for keels between 6 m and 24 m in draft.

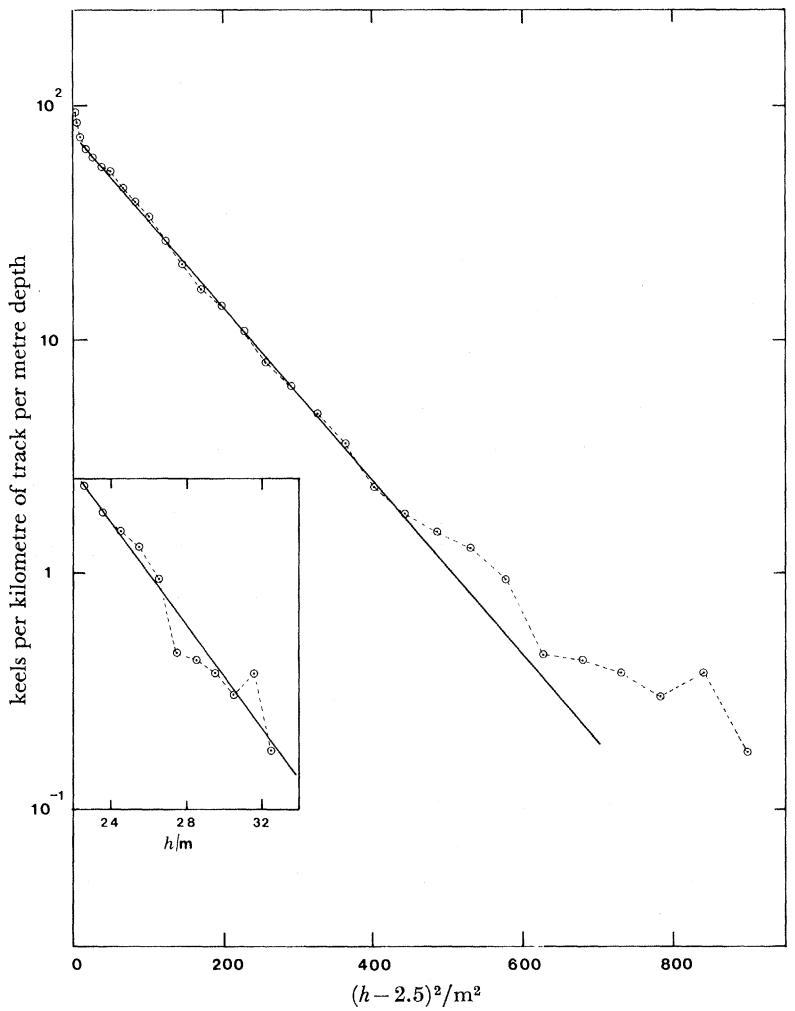

FIGURE 17. Overall distribution of keel drafts h, with number plotted against $(h-2.5)^2$ on semilogarithmic scale.

Wadhams (1980) showed similar curves for the first ten sections and for individual 100 km sections, all of which fitted (10). We expect a deviation for keels shallower than 6 m, because of the presence of deeper floe bottoms in the statistics. However, there is also a significant deviation from theory for keels deeper than 24 m. This was noted by Wadhams (1978*a*) for keels beyond 30 m, although the absolute number of keels in that data set was too small to demonstrate statistical significance. In our case the keel draft distribution beyond 24 m draft actually gives a reasonably good fit to (12), as is shown by the inset to figure 17.

The transition from (10) to (12) at deep drafts can be explained by a modification to the H.W.M. theory. H.W.M. assumed that all keels are geometrically congruent, i.e. have the same slope. Instead we could assume that keels of a given cross-sectional area possess a distribution of slopes around some mean value. Using cross section as the variable for a variational calculation, we would obtain a result which approximates to (10) except at the tail of deepest keels, where only the keels with large slopes appear in the draft distribution. At the extreme depth limit the keel draft will be proportional to slope angle, and the distribution will then approximate to (12).

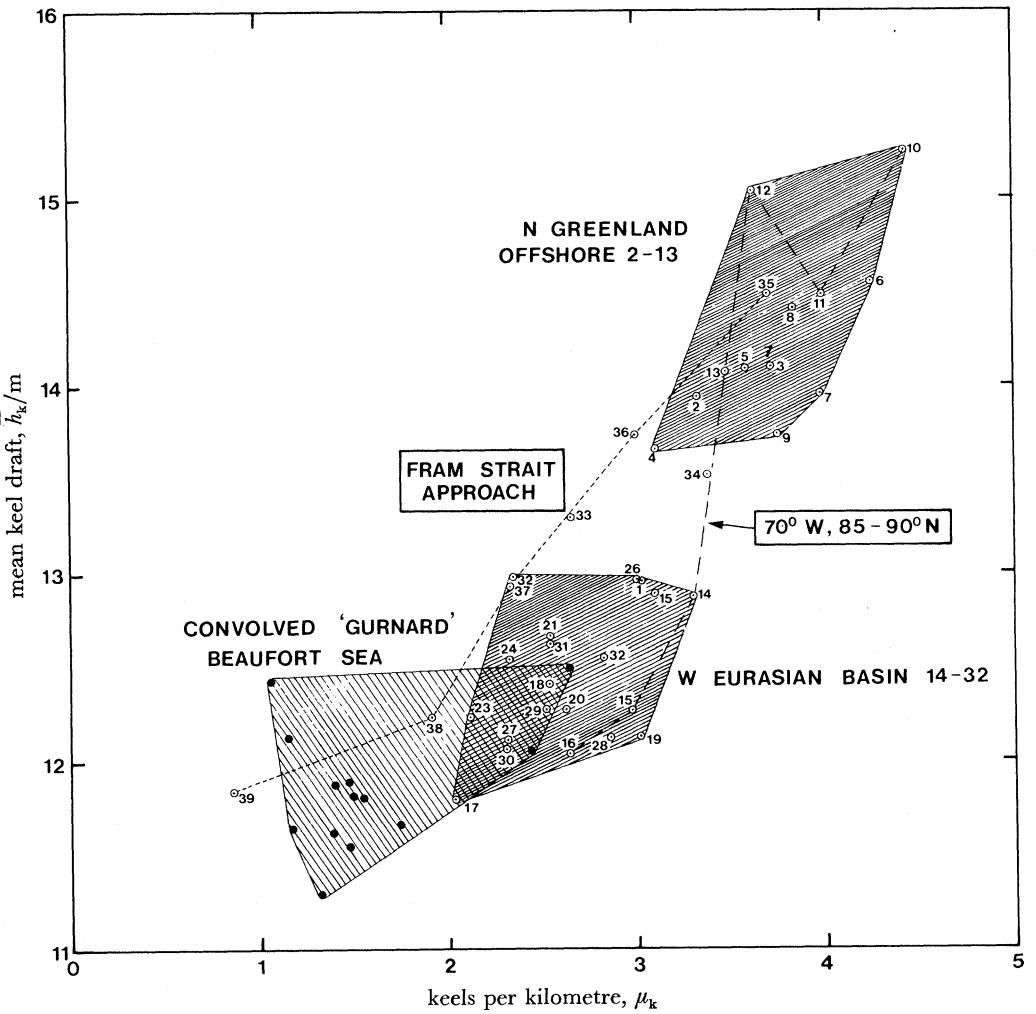

FIGURE 18. Relation between mean keel draft and number of keels per kilometre, for keels deeper than 9 m.

The relation between mean keel draft and the frequency of keels is strongest for deeper keels. Figure 18 shows the result for keels deeper than 9 m. There appears to be a linear relation between the number of keels per kilometre, μ_k, ($h_0 = 9$) and the mean draft, $\bar{h}_k$, with a regression line

$$\bar{h}_k = 1.121\mu_k + 9.81 \quad (r = 0.85). \tag{15}$$

A linear correlation between $\bar{h}_k$ and μ_k was found by H.W.M. for keels deeper than 6 m in data from U.S.S. *Sargo*. Williams *et al.* (1975), however, found no correlation for keels deeper

than 5 m in data from *Dreadnought*. We, too, find no correlation when $h_0 = 5$ m; profiles from the Greenland offshore zone have a higher $\bar{h}_k$ than profiles from the central Arctic régime but with a similar μ_k. Presumably when $h_0 = 5$ the keel frequency is so high that it reaches saturation, i.e. the keel shadowing effect is becoming important, whereas when $h_0 = 9$ keels are sufficiently well spaced for shadowing to be unimportant so that the true correlation can be seen. It is physically reasonable to expect a greater degree of deformation to lead to deeper keels.

Like figures 13 and 14, figure 18 is useful in separating groups of sections in terms of pairs of properties; in this respect it is similar to the (T, S)-diagram in water mass studies. The sections from the north Greenland offshore region all fall within a limited area of the plot, as do the sections from the relatively undeformed central Arctic régime. The dashed line shows the progressive decline in $(\mu_k, \bar{h}_k)$ on the 70° W transect running north to the Pole, while the dotted line shows the radical decline in $(\mu_k, \bar{h}_k)$ as the submarine approaches Fram Strait in sections 35–39.

Comparison of these results with earlier work is possible only for data where ridges are defined similarly. These comprise

(*a*) convolved data from the *Gurnard* cruise in the Beaufort Sea;

(*b*) data from the 1971 *Dreadnought* cruise in the Eurasian Basin.

In figure 18 we have added keel frequencies and mean drafts computed from the *Gurnard* data after convolution of the ice profiles to make them equivalent to a wide-beam profile. It can be seen that the results follow the general trend of the *Sovereign* data, but with a lower μ_k and $\bar{h}_k$ than in the western Eurasian Basin. This is to be expected, since the lower mean ice draft found in the Beaufort Sea suggests that the degree of ice deformation is less there than in the Eurasian Basin. It is possible, however, that the convolution process does not generate a profile with exactly the same characteristics as the *Sovereign* profile. It was found, for instance, that the distribution of keel drafts from the convolved *Gurnard* data still fitted a negative exponential (equation 12) except for the sections that lay in the heavily ridged offshore zone near the Alaskan coast and that obeyed equation (10). This implies either that numerical convolution does not exactly mimic the effect of the *Sovereign's* transducer beamwidth, or else that in a zone of very mild ridging such as the central Beaufort Sea the keel draft distribution still fits (12) even for a wide-beam transducer.

The *Dreadnought* data on keel drafts and frequencies were presented as a scatter diagram of $(\mu_k, \bar{h}_k)$ for $h_0 = 5$ m (Williams *et al.* 1975) by using short lengths of data. The results overlap our own but otherwise give little useful information. However, a table of keel frequencies for $h_0 = 10$ m was also presented, with which we can compare data from *Sovereign* as follows:

latitude range	*Dreadnought* keels per kilometre ($h_0 = 10$)	*Sovereign* keels per kilometre, same latitude range
90–89° N	1.77	1.63
89–88°	1.44	2.05
88–87°	1.70	2.08
87–86°	0.84	2.02
86–85°	1.15	1.85
mean	1.38	1.93

The comparison is not entirely valid, since the *Dreadnought* statistics were computed by using a harsh version of the Rayleigh criterion which used sea level rather than 2.5 m draft as the

zero datum, thus picking out fewer keels. We cannot definitely conclude, therefore, that there was a significantly greater amount of ridging in the Eurasian Basin in October 1976 than in March 1971, but the data do indicate that this is so, especially in latitudes south of 87°.

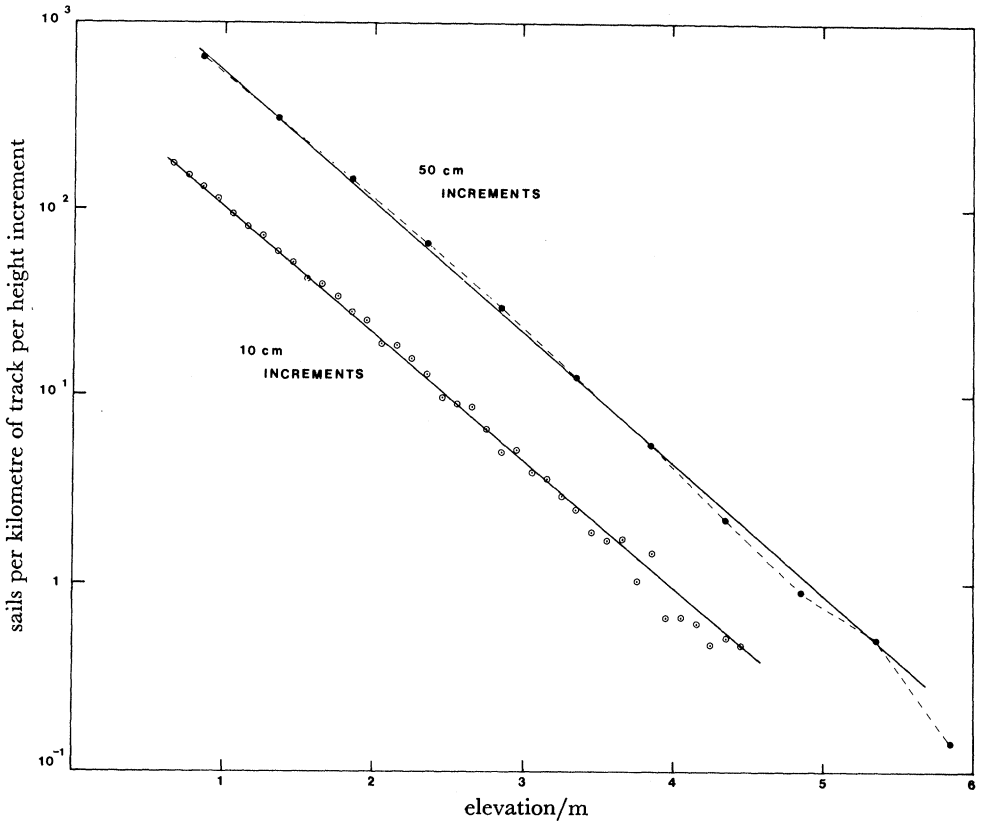

FIGURE 19. Overall distribution of sail heights from the laser profiles, plotted on semilogarithmic scale in 10 cm and 50 cm height increments. Negative exponential distributions of best fit are also shown.

The distribution of sail heights

Figure 19 shows the overall distribution of sail heights from the entire length of the laser profile, plotted in 10 cm height increments. There is an excellent fit to the negative exponential distribution (12). The fit extends from the minimum sail height considered (0.6 m) up to the maximum height in which the numbers of sails per bin are sufficient to merit plotting (10 sails per bin, at 4.5 m). When the data are combined into 50 cm height increments, also shown in figure 19, the fit extends to even greater heights (5.5 m), but there is seen to be a slight yet persistent deviation from a perfect negative exponential, suggesting a law of form $P_r(h) \propto \exp(-\lambda h^p)$, where p is very slightly greater than unity. The deviation is, however, so small that the negative exponential can be taken as the best analytical representation for all practical purposes including predictions of extreme values.

As for keels, there is a clear positive correlation between sail frequency and mean sail height. Figure 20 shows the results for sails exceeding 1 m in height. The north Greenland offshore sections (2–13) and the western Eurasian Basin sections (14–21) occupy well separated areas of the $(\mu, \bar{h})$ diagram. The best linear regression is

$$\bar{h}_s = 0.03725\mu_s + 1.358 \quad (r = 0.78), \tag{16}$$

PHILOSOPHICAL TRANSACTIONS OF THE ROYAL SOCIETY A MATHEMATICAL, PHYSICAL & ENGINEERING SCIENCES

where $\bar{h}_s$ is the mean sail height and μ_s the mean number of sails per kilometre for $h_0 = 1$ m. Such a linear positive correlation was found by Wadhams (1976) for sails in the southern Beaufort Sea in summer, but with a gradient and intercept of 0.0201 and 1.201 respectively for $h_0 = 0.91$ m. Wadhams found, however, that Beaufort Sea ice in winter followed a more complex relation which was not simply linear. We conclude that μ_s and $\bar{h}_s$ are usually positively correlated, but that the form of the correlation is a function of season and ice type.

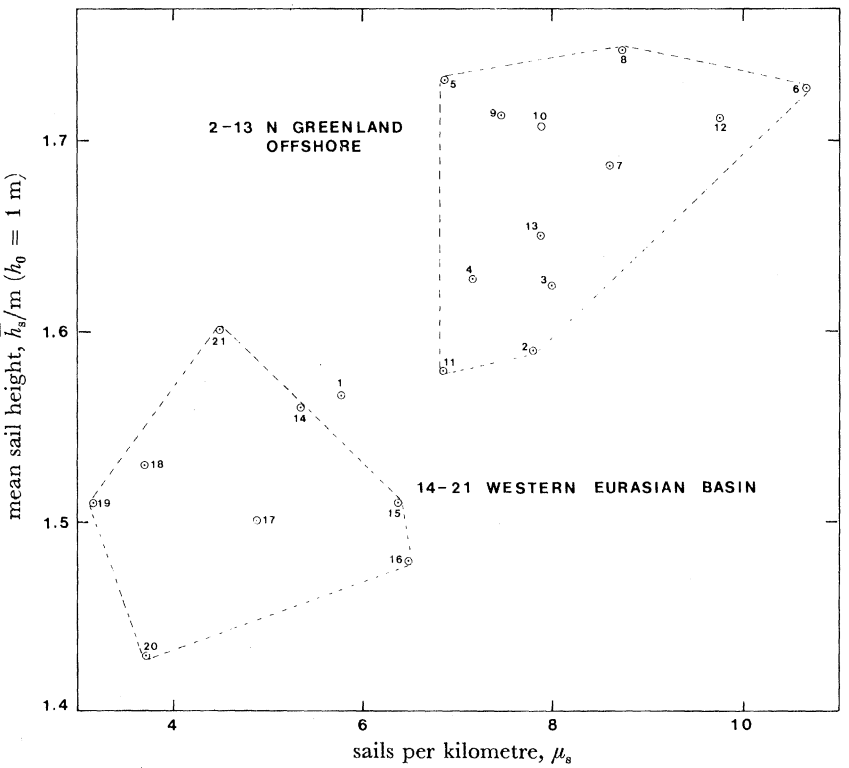

FIGURE 20. Relation between sail frequency and mean sail height, for sails of height exceeding 1 m.

The sail height distribution and the ice elevation distribution are related in that both (figures 11, 19) are negative exponentials. Wadhams & Horne (1980) showed that if sails take an average shape consisting of an isosceles triangle of slope α, then the p.d.f., $P(h)$ of ice elevation beyond some height $h_{\min}$ which excludes undeformed ice is given by

$$P(h)\,\mathrm{d}h|_{h>h_{\min}} = (2\mu_s B \cot\alpha/b)\exp(-bh)\,\mathrm{d}h. \qquad (17)$$

The slope α is less than the true slope because it allows for a variety of track orientations relative to the axes of ridges. We can test the validity of this hypothesis by calculating B, b for each section using (13) and (14), and then finding another 'b' and a value for α from the ice elevation distribution by using (17). The two values of b should agree, and the computed α should be the same for every section. It was found, from analysis of the 21 laser sections, that the mean value of b calculated from sail heights was 1.68 and that calculated from the ice p.d.f. was 1.95, although there was the high correlation of 0.86 between the 21 pairs of values, i.e. they are related systematically. Values of α calculated from (17) were scattered between 4° and 21°, but with a mean of $10.8 \pm 0.7°$. This is close to the value of 11.3° obtained for

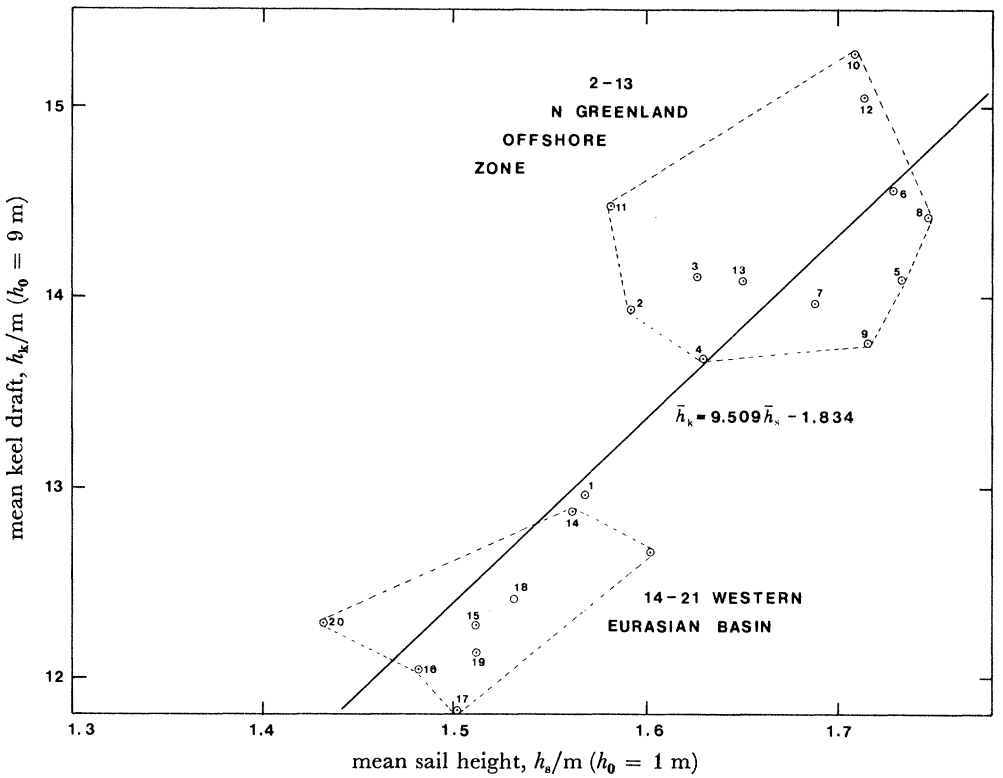

FIGURE 21. Relation between mean keel draft (h_0 = 9 m) and mean sail height (h_0 = 1 m).

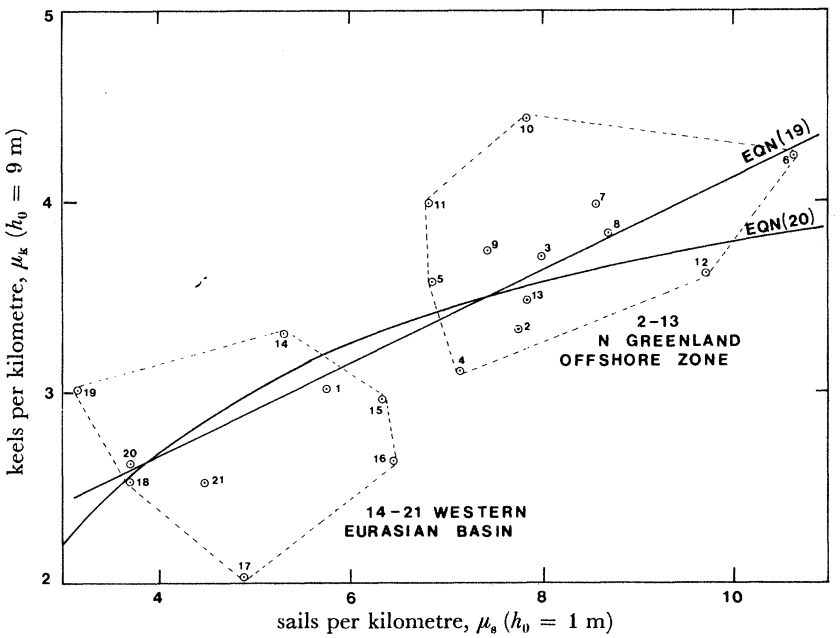

FIGURE 22. Relation between number of keels per kilometre (h_0 = 9 m) and number of sails per kilometre (h_0 = 1 m), with linear and exponential regressions.

Beaufort Sea keels by Wadhams & Horne (1980) in a similar calculation. In our case we cannot extend this analysis to keels, since the wide-beam sonar gives the keel draft distribution a different functional form from the ice p.d.f.

Correlation between keels and sails

We have already shown that with a 100 km length scale there is a good correlation between mean ice elevation and mean ice draft for corresponding sections. We now examine the correspondence between sails and keels. Figure 21 shows the relation between the mean keel draft ($h_0 = 9$ m) and the mean sail height ($h_0 = 1$ m). Despite considerable scatter there is evidence of a linear relation, the regression line being

$$\bar{h}_k = 9.509\bar{h}_s - 1.834 \quad (r = 0.85). \tag{18}$$

Figure 22 shows the relation between the frequency of keels and sails, with the same cut-off values as above. Again there is evidence of a linear relation with a regression

$$\mu_k = 0.2421\mu_s + 1.688 \quad (r = 0.76). \tag{19}$$

If, as suggested in Wadhams (1980), we try instead to construct a function of form $\mu_k = c_1 \exp(-c_2/\mu_s)$, which is thereby forced to pass through the origin and which accounts for a notional saturation of ridging on the underside caused by overlap of keels, we obtain the result

$$\mu_k = 4.735 \exp(-2.279/\mu_s) \quad (r = 0.68). \tag{20}$$

Both of these functions are drawn on figure 22 and it is clear that the simple linear relation fits the data better. The requirement for a line of best fit to pass through the origin is not strictly necessary, since the use of cut-off values implies the possibility of finding an icefield in which there are sails but no keels or vice versa. It should be noted that an error has been detected in the program used to analyse sails for Wadhams (1980), making table 2, figures 12 and 13 and equations 12 and 13 in that paper erroneous.

By using equations (18) and (19) it is therefore possible to convert a distribution of sails computed from a laser profile into a distribution of keels. This is a worthwhile procedure, since recent experiments have shown (Tucker *et al.* 1979; Weeks *et al.* 1980) that it is possible to keep track of how the state of ice deformation over an Arctic offshore province varies with distance from the coast, with downstream distance, with season, and from year to year, all by use of a laser profilometer mounted in a light aircraft. By converting these laser results, which are essentially *comparative* figures, into keel depths and frequencies, an *absolute* measure of the ice deformation can be obtained, suitable for use in numerical models. The technique of conversion is to take the mean sail height and sail frequency on a cut-off of 1 m, and to obtain the corresponding mean keel draft and keel frequency from (18) and (19). The parameter λ is then computed from (11) and thus the keel draft distribution from (10). As our experimental results have shown (figure 17), additional accuracy is obtained in the lower ranges of keel draft if h, h_0 in (10) and (11) are replaced by $h - 2.5$, $h_0 - 2.5$. The resulting $P_r(h)$ is then valid down to 6 m keel draft, despite being computed from a 9 m cut-off.

Leads and polynyas

The distribution of thin ice in the Arctic Ocean is a parameter of great importance to heat budget calculations, since most of the vertical heat flow occurs through ice less than 1 m thick. It is dealt with most appropriately by means of the ice thickness distribution function $P(h)$. For another class of problems, however, it is desirable to know how the thin ice is distributed spatially in leads and polynyas. The ice in refrozen leads is the raw material from which pressure ridges are built, and so the distribution of leads is of importance to sea ice mechanics; further, practical problems of trafficability (distribution of aircraft landing strips and of polynyas suitable for submarine surfacing) require a knowledge of lead distributions.

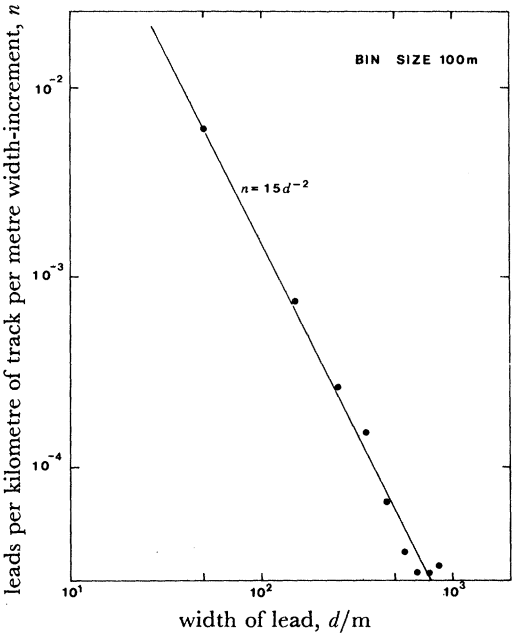

Figure 23. Distribution of widths of leads, from overall submarine track.

For computer analysis a lead was defined as a continuous sequence of depth points (minimum length 5 m) within which no point exceeds 1 m in ice draft. Thus a polynya within which the submarine track intercepts a floe counts as two polynyas, and all leads within a multiple lead system are counted separately. Lead widths were classified in 50 m increments. Figure 23 shows the overall distribution of lead widths for the entire submarine track. If $n(d)$ is the number of leads per kilometre of track per metre increment of width d, then $n(d)$ fits approximately a power law

$$n(d) = 15d^{-2}. \tag{21}$$

This is, however, a very tentative relation which may be specific to this data set, since it did not hold for data from the Beaufort Sea (Wadhams & Horne 1980).

Examining individual sections, we find a very significant clustering in the distribution of wide leads. In the entire track there were 74 leads encountered of width greater than 500 m. Of these, 28 were in the NE Greenland offshore zone (sections 2–13) concentrated especially in the eastern part of it (18 in sections 2–5); only two were in the central Arctic zone of sections 14–31; and no less than 44 were in sections 32–39 where the offshore zone is approached

once again and then merges into the marginal ice zone. Exceptionally large polynyas were nearly all in this last zone; six out of eight that were more than 2 km in width lay in sections 36–39.

Figure 24 is a plot of mean lead width against number of leads per kilometre for each of the 39 sections, with contours representing the percentage of the sea surface occupied by leads.

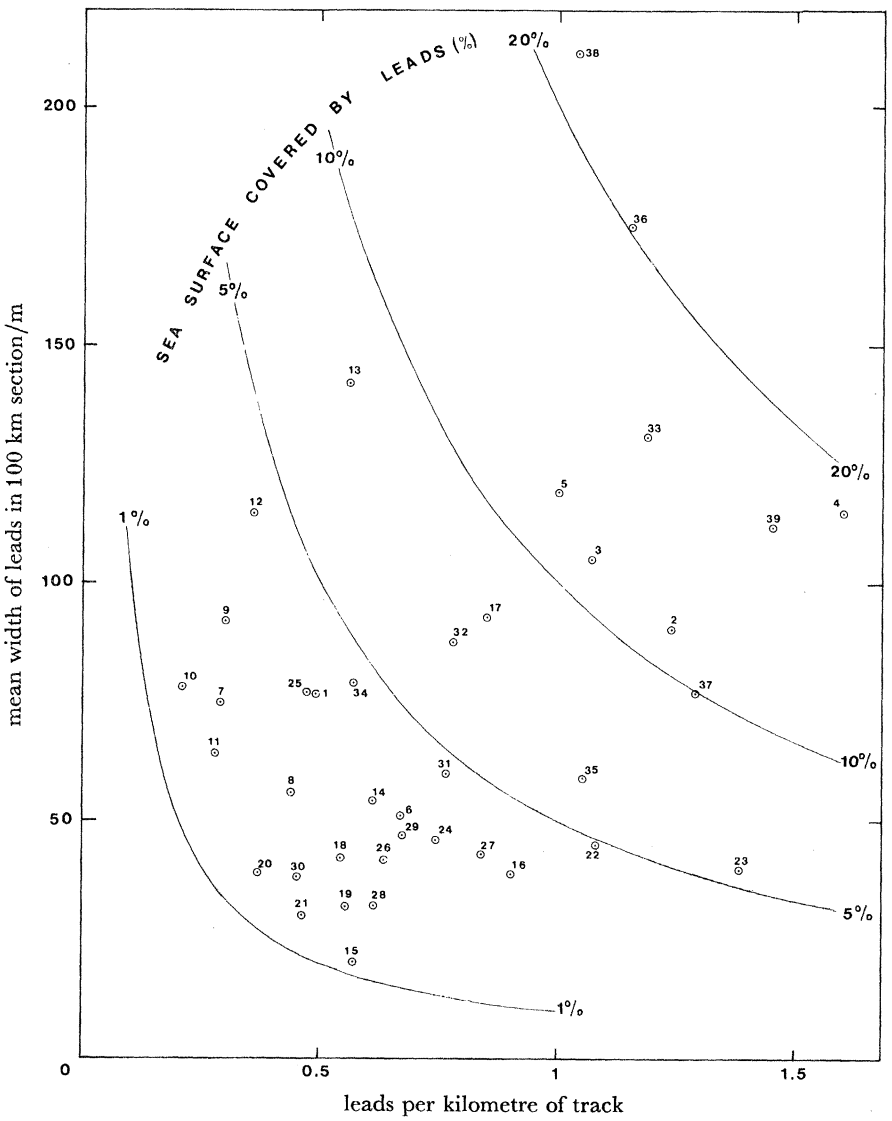

FIGURE 24. Mean lead width plotted against number of leads per kilometre, with contours of percentage of sea surface occupied by leads.

Most sections lie in the range 1–5% leads with between 0.2 and 0.9 leads per kilometre of track. The only sections that contain more than 10% of leads are in the eastern part of the NE Greenland offshore zone (sections 2–5, 33, 36) and in the marginal ice zone (sections 38, 39). The largest percentages of all occur where the Trans-Polar Drift stream is accelerating towards the entrance to Fram Strait (section 38), and in an area off the entrance to Danmarks Fjord where a reduced ice concentration is often observed on satellite pictures (sections 4, 36).

The numbers in figure 24 enable us to make a rough estimate of the degree of accuracy of the thin-ice values in table 3. If the thin ice in a 100 km section of track is divided among n leads, then the true number of leads per 100 km in that type of icefield has a standard deviation of approximately $n^{\frac{1}{2}}$. With numbers of between 20 and 90 we therefore obtain standard deviations of between 11 and 22%. This is a very rough estimate because of the variation in width which also occurs, but it suggests that the thin-ice values in table 3 are reasonably good estimates of the true percentage of thin ice in each section; geographical variations are thus a genuine phenomenon rather than an artefact due to the sampling of small numbers of leads.

Finally, figure 25 is a trafficability diagram showing the widest lead that is likely to be encountered during straight-line transects of different distances across the ice.

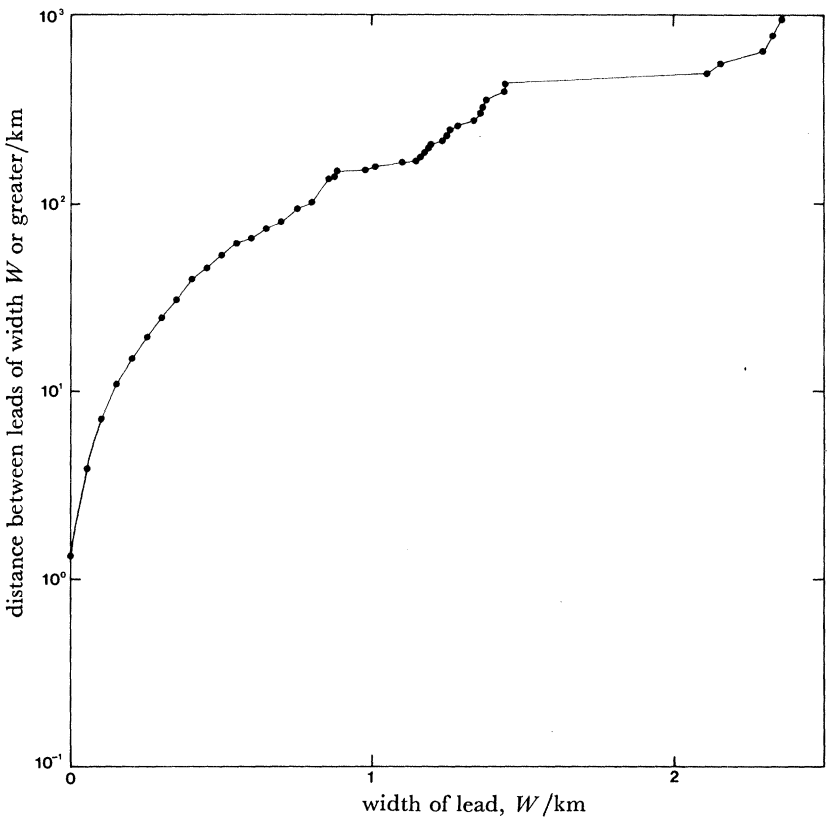

FIGURE 25. A trafficability diagram showing widest lead plotted against distance between encounters, based on data from entire submarine track.

The *Sovereign*–Argus experiment involved the cooperation of many agencies. I wish especially to thank the captain and crew of H.M.S. *Sovereign*; the Hydrographer of the Navy; the Admiralty Underwater Weapons Establishment, Portland; Miss Moira Dunbar and the staff of Defence Research Establishment and Communications Research Centre, Ottawa; and the officers and crew of Maritime Proving and Evaluation Unit, Canadian Forces. I am grateful to Raymond J. Horne for assistance in data analysis. It is a pleasure to acknowledge the support of the Natural Environment Research Council and the continuing support of the Office of Naval Research under contracts N00014-76-C-0660, N00014-78-G-0003 and N00014-80-G-0002.

References

Ackley, S. F., Hibler, W. D. III, Kugzruk, F., Kovacs, A. & Weeks, W. F. 1974 Thickness and roughness variations of Arctic multiyear sea ice. *AIDJEX Bull.* **25**, 75–96.

Bendat, J. S. & Piersol, A. G. 1971 *Random data: analysis and measurement procedures*. New York: Wiley.

Coon, M. D. 1980 A review of AIDJEX modelling. In *Sea ice processes and models* (ed. R. S. Pritchard), pp. 12–27. Seattle: University of Washington Press.

Dunbar, M. 1978 Interpretation of ice imagery from original and modified versions of a real-aperture SLAR. Defence Res. Establ. Ottawa, Rep. 770 (36 pp.).

Dunbar, M. 1979 Fall ice drift in Nares Strait as observed by Sideways-Looking Airborne Radar. *Arctic* **32** (4), 283–307.

Harrison, C. H. 1970 Reconstruction of subglacial relief from radio-echo sounding records. *Geophysics* **35**, 1099–1115.

Hibler, W. D. III 1972 Removal of aircraft altitude variations from laser profiles of the Arctic ice pack. *J. geophys. Res.* **77**, 7190–7195.

Hibler, W. D. III 1979 A dynamic thermodynamic sea ice model. *J. phys. Oceanogr.* **9**, 815–846.

Hibler, W. D. III, Weeks, W. F. & Mock, S. J. 1972 Statistical aspects of sea ice ridge distributions. *J. geophys. Res.* **77**, 5954–5970.

Hibler, W. D. III, Mock, S. J. & Tucker, W. B. 1974 Classification and variation of sea ice ridging in the western Arctic Basin. *J. geophys. Res.* **79**, 2735–2743.

Holyer, I. J. J., Wadhams, P. & Lowry, R. T. 1977 An interactive graphics system for the reduction of airborne laser profiles of sea ice. Scott Polar Res. Inst., Cambridge, Sea Ice Group Tech. Rep. 77–1 (26 pp.).

Ketchum, R. D. Jr. 1971 Airborne laser profiling of the Arctic pack ice. *Remote Sensing Environ.* **2**, 41–52.

Kozo, T. L. & Diachok, O. I. 1973 Spatial variability of topside and bottomside ice roughness and its relevance to underside acoustic reflection loss. *AIDJEX Bull.* **19**, 113–122.

Kozo, T. L. & Tucker, W. B. III 1974 Sea ice bottomside features in the Denmark Strait. *J. geophys. Res.* **79**, 4505–4511.

Leppäranta, M. 1981 Statistical features of sea ice ridging in the Gulf of Bothnia. Winter Navigation Research Board, Helsinki, Tech. Rep. no. 32 (46 pages).

LeSchack, L. A. & Chang, D. C. 1977 Arctic under-ice roughness. Tech. Rep., Development & Resources Transportation Co., 116–1111 University Blvd. W, Silver Spring, Maryland, U.S.A.

Lowry, R. T. & Brochu, C. J. 1978 An interactive correction and analysis system for airborne laser profiles of sea ice. *Can. J. Remote Sensing* **4**, 149–160.

Lowry, R. T. & Wadhams, P. 1979 On the statistical distribution of pressure ridges in sea ice. *J. geophys. Res.* **84**, 2487–2494.

Lyon, W. K. 1961 Ocean and sea-ice research in the Arctic Ocean via submarine. *Trans. N.Y. Acad. Sci.* SER. 2, **23**, 662–674.

Maykut, G. A. 1978 Energy exchange over young sea ice in the central Arctic. *J. geophys. Res.* **83**, 3646–3658.

Maykut, G. A. & Untersteiner, N. 1971 Some results from a time dependent thermodynamic model of sea ice. *J. geophys. Res.* **76**, 1550–1575.

Mock, S. J., Hartwell, A. D. & Hibler, W. D. III 1972 Spatial aspects of pressure ridge statistics. *J. geophys. Res.* **77**, 5945–5953.

Reimnitz, E., Toimil, L. & Barnes, P. 1977 Arctic continental shelf processes and morphology related to sea ice zonation, Beaufort Sea, Alaska. *AIDJEX Bull.* **36**, 15–64.

Rothrock, D. A. & Thorndike, A. S. 1980 Geometric properties of the under side of sea ice. *J. geophys. Res.* **85**, 3955–3963.

Swithinbank, C. W. M. 1972 Arctic pack ice from below. In *Sea Ice*, Proc. Int. Sea Ice Conf., Reykjavik, May 1971 (ed. T. Karlsson), pp. 246–254. National Research Council of Iceland.

Thorndike, A. S., Rothrock, D. A., Maykut, G. A. & Colony, R. 1975 The thickness distribution of sea ice. *J. geophys. Res.* **80**, 4501–4513.

Tucker, W. B. III, Weeks, W. F. & Frank, M. 1979 Sea ice ridging over the Alaskan continental shelf. *J. geophys. Res.* **84**, 4885–4897.

Wadhams, P. 1976 Sea ice topography in the Beaufort Sea and its effect on oil containment. *AIDJEX Bull.* **33**, 1–52.

Wadhams, P. 1977 A British submarine expedition to the North Pole, 1976. *Polar Record*, **18**, 487–491.

Wadhams, P. 1978*a* Characteristics of deep pressure ridges in the Arctic Ocean. *Proc. 4th Int. Conf. Port Ocean Engng under Arctic Conditions*, St. John's, 26–30 Sept 1977 (ed. D. B. Muggeridge), vol. 1, pp. 544–555. Memorial University of Newfoundland, St John's.

Wadhams, P. 1978*b* Sidescan sonar imagery of sea ice in the Arctic Ocean. *Can. J. Remote Sensing*, **4**, 161–173.

Wadhams, P. 1980 A comparison of sonar and laser profiles along corresponding tracks in the Arctic Ocean. In *Sea ice processes and models* (ed. R. S. Pritchard), pp. 283–299. Seattle: University of Washington Press.

Wadhams, P., Gill, A. E. & Linden, P. F. 1979 Transects by submarine of the East Greenland Polar Front. *Deep-Sea Res.* **26**, 1311–1328.

PHILOSOPHICAL TRANSACTIONS OF THE ROYAL SOCIETY A MATHEMATICAL, PHYSICAL & ENGINEERING SCIENCES

Wadhams, P. & Horne, R. J. 1980 An analysis of ice profiles obtained by submarine sonar in the Beaufort Sea. *J. Glaciol.* **25**, 401–424.

Wadhams, P. & Lowry, R. T. 1977 A joint topside-bottomside remote sensing experiment on Arctic sea ice. *Proc. 4th Can. Symp. Remote Sensing*, Quebec, 16–18 May 1977, pp. 407–423. Ottawa: Canadian Remote Sensing Society.

Walker, E. R. & Wadhams, P. 1979 Thick sea-ice floes. *Arctic* **32**, 140–147.

Weeks, W. F., Tucker, W. B. III, Frank, M. & Fungcharoen, S. 1980 Characterization of the surface roughness and floe geometry of the sea ice over the continental shelves of the Beaufort and Chukchi Seas. In *Sea ice processes and models* (ed. R. S. Pritchard), pp. 300–312. Seattle: University of Washington Press.

Westhall, V. H. & Li, H. 1976 An analysis of sea ice bottomside data in the Denmark Strait. *AIDJEX Bull.* **31**, 101–114.

Williams, E., Swithinbank, C. W. M. & Robin, G. de Q. 1975 A submarine sonar study of Arctic pack ice. *J. Glaciol.* **15**, 349–362.

PHILOSOPHICAL TRANSACTIONS OF THE ROYAL SOCIETY A MATHEMATICAL, PHYSICAL & ENGINEERING SCIENCES

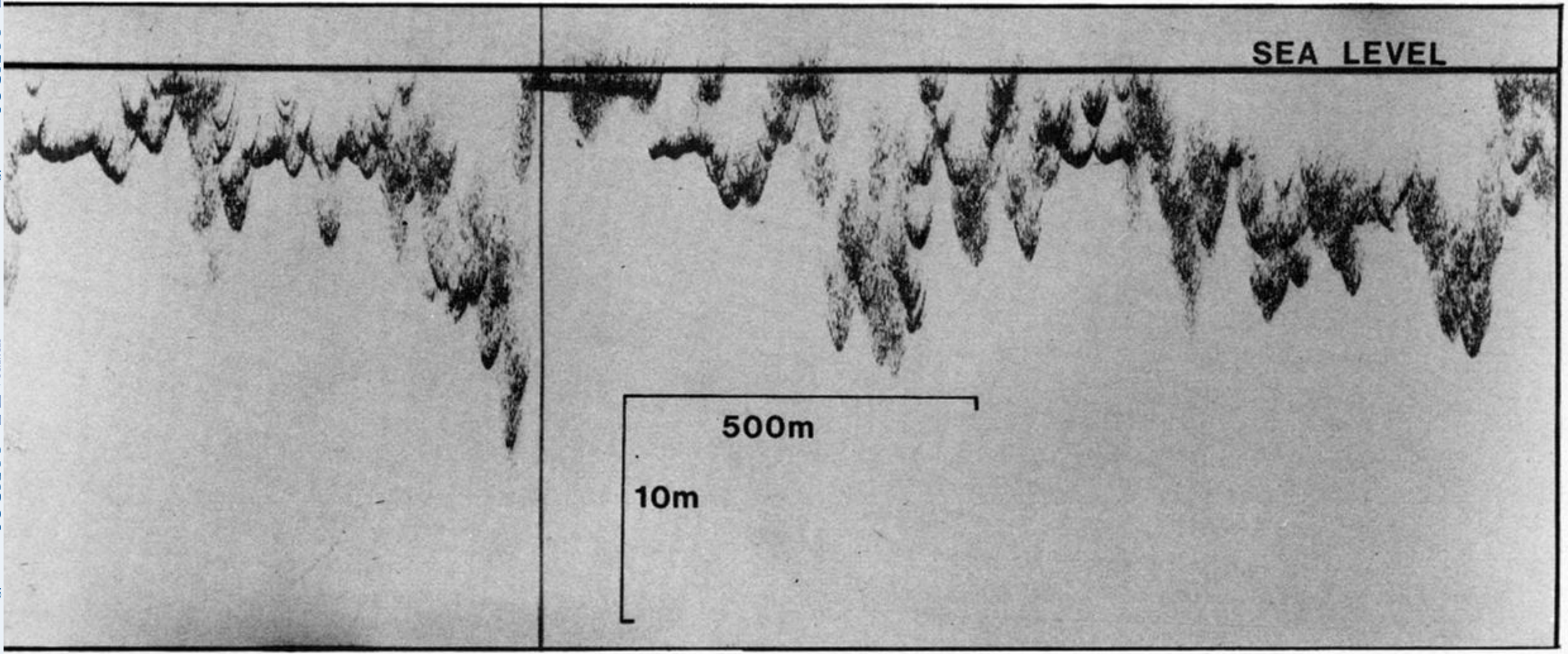

FIGURE 2. A section of under-ice profile.

PHILOSOPHICAL TRANSACTIONS OF THE ROYAL SOCIETY A